NTNU

Norwegian University of
Science and Technology

Magnetic vortex dynamics in interacting micromagnets

Mira Thoen Feiring

Nanotechnology
Submission date: December 2015
Supervisor: Jostein Grepstad, IET
Co-supervisor: Erik Folven, IET
Sam Sloëtjes, IET

Norwegian University of Science and Technology
Department of Electronics and Telecommunications

Abstract

We have studied magnetic vortex oscillations in circular LSMO ($La_{0.7}Sr_{0.3}MnO_3$) disks by micromagnetic simulations. The simulations were performed using the MuMax3 software developed at the DyNaMat group (Dynamics of Functional Nano Materials) at Ghent University.

A magnetic vortex confined in a magnetically soft ferromagnet with micron-sized lateral dimensions possesses a characteristic dynamic excitation known as the translational mode. Initial simulations focused on investigating this rotation of a vortex core around its equilibrium position. Calculations of the eigenfrequencies, extracted through a Fourier transform of the temporal oscillations of the average magnetization distribution, proved to be in agreement with analytical predictions.

Further simulations focused on investigating vortex-vortex interactions, in order to verify the analogy with electrostatics predicted by condensed matter theory. This was done by mapping the respective trajectories of two vortices confined in two overlapping micron-sized disks. A rudimentary method for quantifying this interaction was introduces, based on aspect ratio of the horizontal and vertical diameters of a given trajectory.

Comparing the trajectories for vortices with different rotational modes, as well as for different center-to-center distances between the ferromagnetic disks, a repulsive interaction was verified.

Sammendrag

Vi har studert oscillasjoner av magnetiske virvler (vortices) i sirkulære disker av LSMO ($La_{0.7}Sr_{0.3}MnO_3$) ved hjelp av mikromagnetiske simuleringer. Disse simuleringene ble utført med programmet MuMax3 som er utviklet av DyNaMat-gruppen (Dynamics of Functional Nano Materials) ved Universitetet i Gent.

I magnetisk myke ferromagneter med laterale dimensjoner på mikrometernivå, vil magnetiske virvler inneha en karakteristisk dynamisk eksitasjon kjent som den translasjonelle moden. For de initielle simuleringene lå fokuset på å studere denne rotasjonen av en virvel-kjerne rundt likevektsposisjonen. Egenfrekvensen til den translasjonelle moden kan beregenes ved en Fouriertransformasjon av den gjennomsnittlige romlige magnetiseringen over tid, of resultatene stemte her overens med den analytiske modellen.

Videre simuleringer fokuserte på å undersøke interaksjoner mellom to virvler, for å verifisere analogien til elektrostatikk slik den er gitt teoretisk i kondenserte fasers fysikk. Dette ble gjort ved å kartlegge rotasjonsbanene til to virvler i en struktur bestående av to overlappende disker med dimensjoner på mikrometernivå. En enkel metode for å kvantisere denne interaksjonen ble introdusert, basert på størrelsesforholdet mellom den horisontale og den vertikale diameteren i en gitt rotasjonsbane.

Ved å sammenligne banene til virvler med ulik rotasjonell mode, samt for ulike avstander mellom diskenes senter, kunne en frastøtende interaksjon bekreftes.

Preface

This thesis is written for the degree of Master of Science at the Norwegian University of Science and Technology. The work presented herein has been performed during the autumn of 2015 with the Oxide Electronics group of the Department of Electronics and Telecommunications.

I would like to thank Prof. Jostein Grepstad and Assoc. Prof. Erik Folven, for giving me a very interesting thesis project. I would also like to extend my deepest gratitude to Sam Slöetjes for invaluable assistance, both with the simulation software, and in many fruitful discussions.

Finally, I would like to thank Andreas Nordahl for continuing to motivate me, and for much help with the final proofreading.

Contents

List of Figures

Chapter 1

Introduction

1.1 Motivation

In 1965, Gordon E. Moore predicted that the number of transistors per integrated circuit for minimum cost would reach 65,000 by 1975, implying that the number would double every other year [5]. The observation proved accurate, and the trend has since been termed "Moore's Law". The main reason for its continued accuracy is the fact that the electronics industry has employed the law as a guideline when determining long-term goals.

In accordance with Moore's law, the computer industry has seen exponential improvements over the last 50 years. However, we are now reaching a point where the size of a transistor is measured in the number of atoms it is made up of, and it is clear that this continued downsizing will not be possible for much longer. As a result, there is extensive research going into searching for the new technologies that can continue to power the growth of the electronics/computer industry.

With the discovery of the giant magnetoresistive effect (GMR) in 1988, a new field of spin-based electronics (spintronics) was born [6]. In contrast with silicon-based transistors, the information carrier in spintronic devices is the electron spin, rather than the electron charge.

Since the first commercial silicon transistor was introduced in 1954 [7], there has been extensive research and investments going into that field of study. Consequently, there is much research on alternative silicon-based technologies, that will allow further downscaling of integrated circuits. It is therefore unlikely that a any new, emerging technology will beat silicon-based structures in every performance category. However, logic devices based on magnetism hold one very important advantage over todays charge-based architecture, and that is related to power consumption. While charge-based logic devices are volatile, meaning that a power supply is needed to maintain the logic state, a logic device based on magnetism is nonvolatile, thus requiring no energy in stand-by

mode. Research also suggests that the intrinsic switching energy of a magnetic device will be much lower than a charge-based transistor [8].

Recent developments in nanofabrication and precise measurement techniques have enabled us to study laterally confined nanoscale magnetic structures [9]. Among them, patterned nanomagnets are promising candidates for high density magnetic data storage devices, magnetic field sensors, magnetic random access memory (MRAM), etc.

As the advances in nanofabrication and precise measurement techniques have increased our insight on nanomagnetism, investigations on magnetic vortices, stabilized in circular nanodisks, have drawn much attention both experimentally and theoretically [9]. Vortices appear in such magnetic structures due to geometrical confinement that alters their energetics [3].

These magnetic configurations possess magnetization cores with a diameter of a few nanometers pointing out-of-plane with a surrounding in-plane magnetization pattern. As such, a vortex is characterized by two binary properties, so-called "topological charges", a chirality (counter-clockwise or clockwise direction of the in-plane rotating magnetization) and a polarity (the up or down direction of the vortex core's magnetization), each of which suggests an independent bit of information in future high-density nonvolatile recording media [10].

1.2 Background

Magnetic vortices are typically the ground state in geometrically confined ferromagnets with small magnetocrystalline anisotropy. Although the magnetic vortex state was theoretically predicted several decades ago, it has recently received renewed attention since it is often found to be the ground state of nano-patterned magnetic particles. A substantial number of the publications exist where the stability of the vortex state has been investigated with regard to the sample shape, size and also the presence of an external field [3].

A magnetic vortex confined in patterned ferromagnetic thin films with micron-sized lateral dimensions possesses a characteristic dynamic excitation known as a translational mode, characterized by a spiral-like precession of the vortex core around its equilibrium position [11]. This translational mode was predicted theoretically in 2002 by Guslienko *et al.* [12], and later observed experimentally by Park *et al.* [13] using a time-resolved Kerr effect technique. It has since been studied intensively, both analytically and experimentally.

Various properties of the magnetic vortex have been investigated, such as its stability, the eigenfrequency of the translational mode, switching of the vortex core polarity, etc. For example, theoretical analysis on the dynamics of the off-centered vortex have shown that the rotational direction of the circular motion around the disk center depends exclusively on the direction of the core polarization [14].

1.3 Project outline

In this thesis the dynamics of vortices confined in thin film ferromagnetic disks is investigated by micromagnetic simulations. A general study of a the properties of a vortex confined to a single disk is presented, as well as an investigation into the effect of varying different material parameters on the translational mode. Furthermore, a study into the interaction between two vortices confined in two overlapping disks will be presented.

Theories of condensed matter physics suggests that magnetic vortices can be considered as positive and negative point charges of unit strength [15], by virtue of their topological charge. Although much research has been done investigating the interaction between two vortices confined in laterally separated nanomagnets, there has been few studies investigating the analogy to electrostatics. Such a study will be presented in this paper, providing a novel method for measuring the vortex-vortex repulsion.

This thesis consists of five chapters. After this introduction, Chapter 2 gives a short theoretical introduction to magnetic phenomena in solid materials, with focus on aspects regarding the magnetic vortex state. Chapter 3 gives an overview of the methods of modeling and analysis, as well as an introduction to the simulation software used. Chapter 4 covers the results from the various simulations, and the conclusions are summarized in Chapter 5.

Chapter 2

Theory

2.1 Magnetic materials

From classical electromagnetism, we know that magnetism arises from the angular momentum of a charged body. On the atomic level, magnetism is results from the orbital and intrinsic angular momentum (or spin) of electrons [16]. Due to these properties an electron behaves like a small magnetic dipole, with a magnetic moment $\mathbf{m}$. Indeed, the nucleus also has a magnetic moment, but its strength is negligible compared to that of the electron [17].

The magnetic moment of an atom depends on the vector sum of all its electronic moments. A material composed of atoms where the magnetic moments of all electrons cancel out one another, is diamagnetic. On the other hand, if the cancellation of the electronic moments is only partial, such that the net magnetic moment is nonzero, the material is para-, ferro-, antiferro- or ferrimagnetic [17].

The magnetization $\mathbf{M}$ of a material is the sum of the magnetic moments of all the atoms in the material. However, the magnetic properties of a material are not only characterized by the magnitude and direction of this magnetization, but also by how $\mathbf{M}$ varies in response to an applied magnetic field $\mathbf{H}$. In many materials, $\mathbf{M}$ and $\mathbf{H}$ are proportional [18]:

$$\mathbf{M} = \chi_m \mathbf{H} \tag{2.1}$$

The proportionality constant χ_m is called *magnetic susceptibility*. In this kinds of linear material, the flux density $\mathbf{B}$ is proportional to $\mathbf{H}$:

$$\mathbf{B} = \mu_0(\mathbf{H} + \mathbf{M}) = \mu_0(1 + \chi_m)\mathbf{H} = \mu_r \mu_0 \mathbf{H} = \mu \mathbf{H} \tag{2.2}$$

Here μ is the absolute magnetic permeability, μ_0 the permeability in vacuum and $\mu_r = (1 + \chi_m)$ is the relative permeability [18].

Plotting **M** as a function of **H**, we obtain what is called a magnetization curve. For dia-, para-, and antiferromagnetic materials such a curve will be linear. Ferro- and ferrimagnetic materials, on the other hand, behave differently, as the magnetization **M** depends not only on the applied field, but also the history of said field [18]. In ferro- and ferrimagnetic materials it is often more useful to study the total flux density **B** produced by a given field, given by the permeability μ [17]. In general, diamagnetic materials are characterized by $\mu_r < 1$, while para- and antiferromagnetic materials will have $\mu_r > 1$. That is, these materials are linear with $\mu_r \sim 1$. In ferro- and ferrimagnetic materials, both μ_r and χ_m are large and positive, as well as being dependent on **H** [17].

Para-, dia- and antiferromagnetic materials are characterized by a small (absolute) susceptibility, compared to ferro- and ferrimagnetic materials. Even when a field is applied, thermal agitation of the atoms opposes the tendency of the atoms to align with the direction of the field, resulting in only partial alignment. An increase in temperature will increase the randomizing effect of thermal agitation, leading to a decrease in the susceptibility [17].

2.1.1 Domains and magnetic anisotropy

The reason for the large value of χ_m in ferromagnetic materials is a long-range ordering of their atomic moments, even in the absence of an external field [16]. That is, ferromagnets possess a nonzero spontaneous magnetization. This spontaneous magnetization results from, and is stabilized by, strong interatomic interactions known as exchange coupling. Ferromagnets are also subject to thermal agitation, but below a certain temperature known as the Curie temperature T_C the exchange coupling will dominate. Above T_C, thermal disorder reigns, leading to a vanishing of the spontaneous magnetization and effectively causing a ferromagnetic material to become paramagnetic [19].

However, a large region of ferromagnetic material with a uniform magnetization will create a large magnetic field extending into the space outside the material (known as a demagnetization field). Maintaining such an external field requires substantial magnetostatic energy. This energy can be reduced by flux closure and domain formation (fig. 2.1) [19]. Domains are regions in a ferromagnetic material that are spontaneously magnetized to the saturation value M_s, meaning that all available atomic moments are aligned parallel to one another. If the direction of magnetization in the various domains are aligned so as to cancel one another out, the material effectively has no net magnetization [17].

The boundary separating two domains is called a domain wall. Domains and domain walls are created in order to minimize the magnetostatic energy. However, if the magnetization direction were to change abruptly from $0\,^\circ$ to $180\,^\circ$ between two adjacent

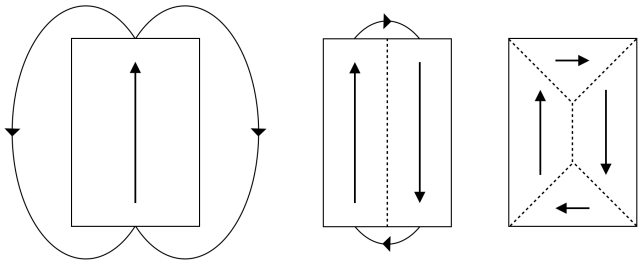

FIGURE 2.1: *Flux closure by domain formation*

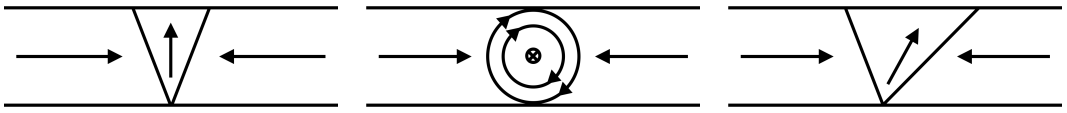

FIGURE 2.2: *Domain wall structure in magnetic thin film nanowires with longitudinal magnetization. (a) (symmetric) transverse wall, (b) vortex wall, (c) asymmetric transverse wall. Figure adapted from [1].*

domains there would be a large energy cost due to the exchange interaction, which favors parallel alignment of neighboring spins. Reduction of the exchange energy can be achieved by distributing the 180 ° rotation over several interatomic spacings, minimizing the angle between adjacent spins [16].

Except in special cases, by virtue of their limited thickness, the magnetization in thin films lies in the plane of the film, because a large demagnetizing field would be imposed normal to the plane of the film if **M** were oriented in that direction. Consequently, the demagnetizing field in the plane of the film is nearly zero [17].

In thin films with limited width, the magnetization will typically align with the longitudinal direction of the film. If two domains with anti-parallel magnetization meet, a domain wall with a 180 ° rotation of the field contained in the plane of the film is required. The wall structure can be either a (symmetric) transverse wall, a vortex wall, or an asymmetric transverse wall, depicted in figure 2.2 [1].

In ferromagnetic materials, the field needed to magnetize a sample to saturation depends on which crystallographic direction the field is applied along. This preference for the magnetization to lie in a certain direction, known as the *easy axis*, is called magnetic anisotropy, and it can originate from the sample shape, crystaline symmetry, strain, or directed atomic pair ordering [16]. The only kind of magnetic anisotropy intrinsic to a material is the so-called magnetocrystalline anisotropy [17], which involves electrostatic crystal-field interaction as well as relativistic spin-orbit coupling.

Shape anisotropy also has an important effect on the magnetization of a material, especially as the dimensions become smaller. A nonspherical magnetic material will be

more easily magnetized along a long axis than along a short axis, as the demagnetizing energy will be higher along the short axes [17].

Depending on the material, a ferromagnet can have one or multiple easy axes [16]. Thin films of $La_{0.7}Sr_{0.3}MnO_3$ (LSMO) generally have a biaxial magnetic anisotropy, with the easy axis along the $\langle 110 \rangle$ crystal direction, and the hard axis along $\langle 100 \rangle$ [20].

When an external field **H** is imposed on a ferromagnet, the magnetic moments tend to align parallel to the direction of the field so as to minimize the potential energy. This can happen through domain wall motion, serving to expand the volume of those domains having the largest component of **M** parallel to **H**. For weak fields, this process will continue until all domains are magnetized either parallel or at right angles to the direction of the applied field. Further increase of magnetization, in order to obtain saturation, can only be achieved through domain rotation. This process requires stronger fields, as rotation of the magnetization away from an easy axis generally requires more energy than domain wall motion [16].

2.1.2 Magnetization energetics

The energy terms dictating the magnetization texture in a ferromagnetic material are described mathematically by the following relations.

Exchange energy

The exchange interaction is the main contribution to the spontaneous magnetization in ferromagnetic materials. This energy is minimized when there is only a slight variation in the magnetization direction of adjacent spins, given by the equation,

$$E_{ex} = \int_V \frac{A}{M_s} (\nabla \mathbf{M}(\mathbf{r}))^2 dV \tag{2.3}$$

where M_s is the saturation magnetization and A is the so called exchange stiffness. When all spins have the same orientation $\nabla \mathbf{M} = 0$, and consequently the entire integral is zero. The exchange stiffness is a measure of the force tending to keep adjacent spins parallel to one another, that is, the torsional stiffness of the spin-spin coupling [17].

Magnetocrystalline anisotropy energy

The magnetocrystalline anisotropy energy favors configuration where the direction of magnetization is aligned along an easy axis and is given by

$$E_a = \int_V K_1 sin^2(\theta) dV \tag{2.4}$$

where K_1 is the first order (uniaxial) anisotropy constant and θ is the angle between magnetization direction and easy axis. In the case of materials having more than one

easy axis, for example cubic anisotropy, the expression has additional terms [19].

Magnetostatic energy

The magnetostatic energy, also referred to as magnetostatic self-interaction or demagnetizing energy, is the energy required to maintain a magnetization that produces a field outside a sample. This field will effectively try to demagnetize the material, favoring flux closure inside the body of the sample. This energy is influenced by the shape of the sample, as a nonspherical sample is easier to magnetize along a long axis than along a short axis [17]. The magnetostatic energy is given by

$$E_d = -\frac{\mu_0}{2} \int_V \mathbf{M}(\mathbf{r}) \cdot \mathbf{H}_d(\mathbf{r}) dV \tag{2.5}$$

where $\mathbf{H}_d$ is the demagnetization field (self-interaction field) [19].

Zeeman energy

The Zeeman energy will be minimized when the magnetization is aligned parallel to the direction of an applied field [21]. The Zeeman energy is given by

$$E_Z = -\mu_0 \int_V \mathbf{M}(\mathbf{r}) \cdot \mathbf{H}_a dV \tag{2.6}$$

where $\mathbf{H}_a$ is the applied field.

Micromagnetic free energy

The local magnetization is determined by the competition between the interatomic exchange, anisotropy, magnetostatic, and Zeeman energy. It can be obtained by minimizing the micromagnetic free energy, given by [19]

$$E = E_{ex} + E_a + E_d + E_Z \tag{2.7}$$

from which an expression for the effective field can be derived [21]

$$\mathbf{H}_{\text{eff}} = -\frac{1}{\mu_0} \frac{\partial E}{\partial \mathbf{M}} \tag{2.8}$$

At equilibrium the magnetization $\mathbf{M}(\mathbf{r})$ lies everywhere parallel to this field.

2.2 Magnetic vortices

Magnetic vortices are typically the ground state of geometrically confined ferromagnets with small magnetocrystalline anisotropy [3]. The magnetic vortex structure is characterized by an in-plane curling of the magnetization $\mathbf{M}$ around a central region. At the center region, where magnetization vectors would align antiparallel to one another, the magnetization is forced out-of-plane in order to minimize the exchange energy, creating a vortex core magnetized perpendicular to the plane.

2.2.1 Stability of the vortex state

In principle the stability of a vortex structure is determined by minimization of the magnetic energy of the system, which includes the energy terms introduced in section 2.1 [22]. In micron sized, circular ferromagnetic disks, the magnitudes of the exchange, magnetostatic, and magnetic anisotropy energies depend on the sample size and geometry. Consequently, disk radius R and the disk thickness L are parameters important to the vortex stability.

Another important parameter is the exchange length, which describes the length below which the exchange interaction dominates the magnetization structure. The exchange length is defined as:

$$l_{ex} = \sqrt{\frac{2A}{\mu_0 M_s^2}} \tag{2.9}$$

where $\mu_0 = 4\pi \times 10^{-7}\,\mathrm{H/m}$ is the permeability of vacuum. The vortex state is stabilized when $g \equiv L/R \ll 1$ and $R, L \gg l_{ex}$ [9].

Calculations of the geometrical stability of the vortex state were conducted by Metlov and Guslienko [2]. Here, a phase diagram was plotted on the basis of calculations of the vortex state energy and the energies of single-domain states. According to Guslienko [3], the phase diagram is universal for soft magnetic disks if the geometrical sizes (radius and thickness) are normalized to the exchange length l_{ex} (fig. 2.3).

2.2.2 Vortex characterization

A magnetic vortex is a type of topological defect. A topological defect is in general characterized by some core region (e.g., a point or a line) where order is destroyed and a far field region where the order parameter changes slowly with position. Like an electric point charge, its presence can be determined by measurements of an appropriate field on any surface enclosing its core. Topological defects are referred to by different names depending on which symmetry is broken and the particular system in question. In xy-models, in which we consider spins such as magnetic moments to rotate in a plane, they are referred to as vortices [15].

This topological defect is characterized by three topological charges: the polarity p, the chirality c, and the vorticity q (see fig. 2.4). The definition of the former two is fairly straight forward. The polarity defines the relative orientation of the magnetic moments inside the vortex core with respect to the plane of the ferromagnet, and takes the values $p = \pm 1$, $p = +1$ corresponding to $m_z > 0$ and $p = -1$ to $m_z < 0$. The chirality defines the direction of the in-plane curling magnetization, which can be clockwise or counter-clockwise, corresponding to $c = +1$ and $c = -1$ respectively [3].

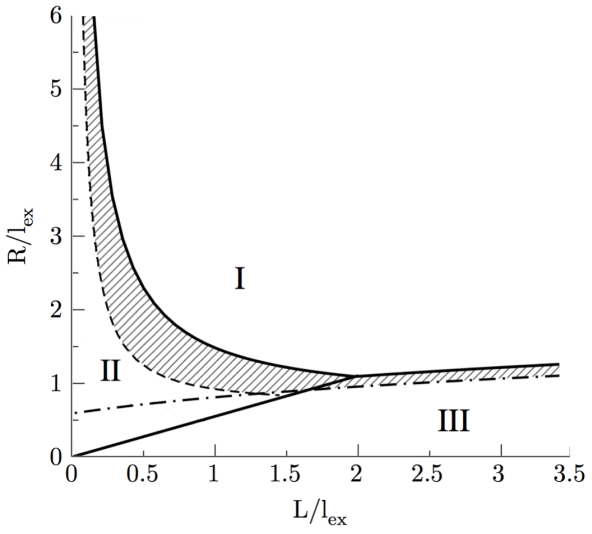

FIGURE 2.3: *Diagram of stability of the vortex state in circular disks with radius R and thickness L (l_{ex} is the exchange length). Three magnetization states are stable: vortex (I), in-plane single domain (II), and perpendicular single domain (III). The energy equilibrium lines are shown as solid lines. The dashed line corresponds to the border of stability of the vortex state. The dot-dashed line corresponds to the equilibrium vortex core radius. The shaded area is a region of bi-stability. Figure adapted from [2].*

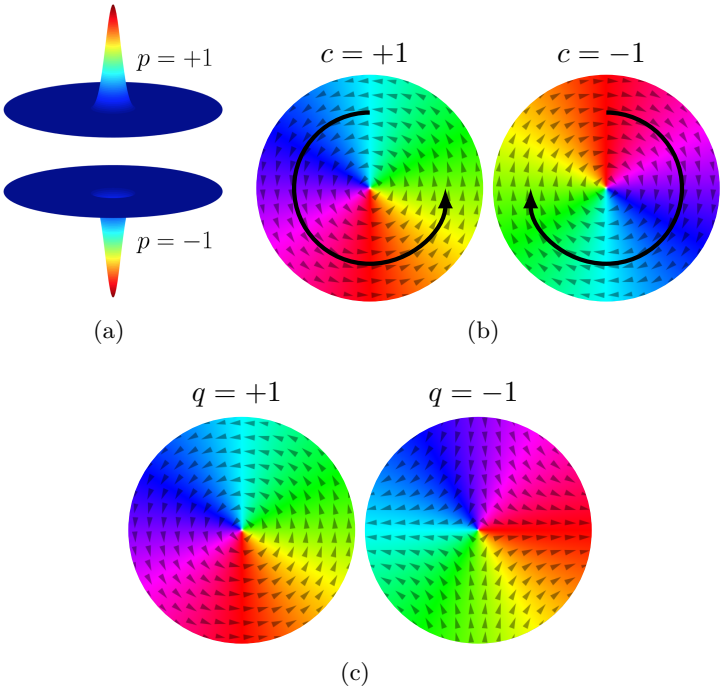

FIGURE 2.4: *Topological charges of a ferromagnetic vortex: (a) polarity, (b) chirality, and (c) vorticity.*

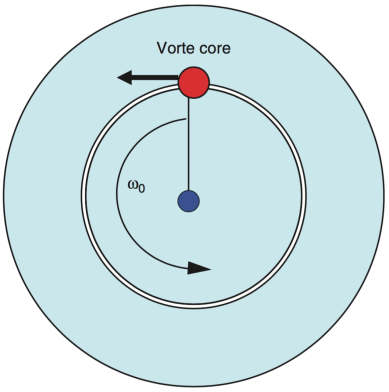

FIGURE 2.5: *Trajectory of the vortex core motion in a circular disk with eigenfrequency ω_0 given by Eq. 2.11, from [3].*

The vorticity can be understood as follows: For 2D ferromagnetic thin films, the order parameter is typically taken as a unit vector of in-plane magnetization, $\hat{\mathbf{m}} = \mathbf{M}/|\mathbf{M}|$. Letting θ be the angle the magnetization vector makes with a given direction, for example the x-axis, the vorticity measures the total angle θ through which the vector $\mathbf{m}(\mathbf{r})$ turns in a circular contour around the core. The quantity q, an integer number of 2π, is also commonly referred to as the *winding number* [22], and is defined mathematically by:

$$q = \frac{1}{2\pi} \oint_{\partial\Omega} \nabla\theta \, \mathrm{d}\mathbf{r} \tag{2.10}$$

q takes integer values (± 1) when Ω, described by the polar coordinate $\mathbf{r}(r, \phi)$, encompasses a topological defect [23]. $q = +1$ is related to a vortex, while $q = -1$ is related to an antivortex [22].

2.2.3 Vortex dynamics

In laterally confined structures such as disks, the vortex core can be seen as trapped in a potential well that forces it to stay at the center. However, if the core is moved away from its equilibrium position, for example by a magnetic field, it will experience a restoring force against this motion. This restoring force arises from the distortion of the circular arrangement of the magnetization, resulting in an internal demagnetizing field opposing the displacement. When the external field is removed, the core gyrates at a given frequency in an orbit around its equilibrium position (fig. 2.5), going back to this position in a spiral motion due to damping (magnetic relaxation in the material). This type of magnetic vortex oscillation is commonly referred to as the vortex translational, or gyrotropic, mode [22].

Analytically, this motion of the core can be described by Thiele's equation:

$$\mathbf{G} \times \frac{d\mathbf{X}}{dt} - \frac{\partial W(\mathbf{X})}{\partial \mathbf{X}} = 0 \tag{2.11}$$

where $\mathbf{X} = (X, Y)$ is the position of the vortex core. $W(\mathbf{X})$ is the potential energy of the shifted vortex, and the second term in this equation thus describes the restoring force acting on the vortex towards its equilibrium position [12].

The first term in Eq. 2.11 is called the *gyroforce* and is determined by the vortex non-uniform magnetization distribution (the vorticity q). This force is proportional to the gyrovector $\mathbf{G} = -G\hat{z}$, where G is the gyroconstant. In the case of ferromagnetic disks of limited thickness the gyroconstant is described by:

$$G = \frac{2\pi}{\gamma} qpLM_s \tag{2.12}$$

where γ is the gyromagnetic ratio, L the thickness of the disk, and q and p the topological charges introduced in section 2.2.2 [3].

Regarding the aspects of vortex dynamics investigated in this thesis, one physical implication of Eq 2.12 is of particular importance. For a vortex of a given vorticity, the sign of the gyroconstant, and consequently the gyrovector, is imposed by the vortex polarity p. Combining this notion with the expression for the vortex gyrotropic motion (Eq. 2.11), it is evident that the direction of rotation of the vortex core is determined solely by the polarity, $p = +1$ corresponding to counter-clockwise (CCW) and $p = -1$ to a clockwise (CW) rotation. Note that the chirality c of the vortex does not influence the dynamics.

The eigenfrequency of the vortex translational mode can be calculated analytically from the following expression, derived from Eq. 2.11 [11],

$$\omega_0(\beta, R) = 2\gamma M_s \left[4\pi F_v(\beta) - \frac{1}{2} \left(\frac{l_{ex}}{R} \right)^2 \right] \tag{2.13}$$

where $\beta = L/R$ is the disk aspect ratio, $F_v(\beta) = \int_0^\infty dtt^-1 f(\beta t) I^2(t)$, $f(x) = 1 - (1 - \exp(-x))/x$, $I(t) = \int_0^1 dx x J_1(x)$, $J_1(x)$ is the first-order Bessel function, and l_{ex} is the exchange length. The full derivation of this expression is beyond the scope of this thesis. However, as this relation has proved to be in good agreement with micromagnetical simulations, it will provide a basis of comparison for our results.

Another important aspect of vortex dynamics is the recently experimentally observed dynamic vortex core reversal. That is, the sudden switch of core polarity in moving vortices. The physics behind this reversal mechanism has since been studied intensively. The most important aspects relating to this thesis will be described briefly.

Investigations by Guslienko, Lee, and Kim [4] has found that the origin of vortex core reversal is a gyrotropic field $\mathbf{h}$. This field is induced by vortex dynamic motion

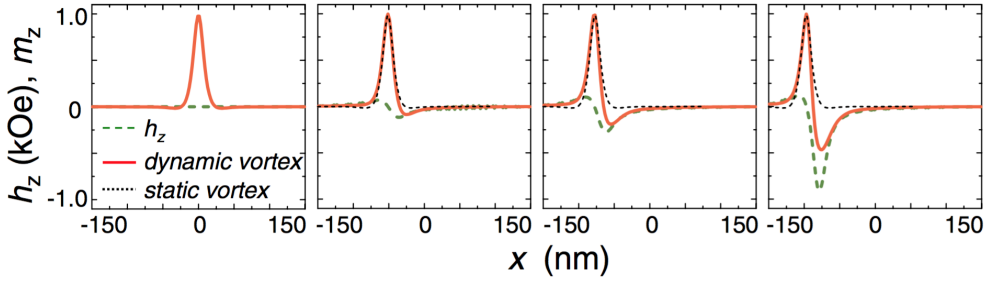

FIGURE 2.6: *Dynamic (solid line) and static (dotted line) vortex core magnetization profiles, as well the gyrofield h_z (dashed line) profile, along a line crossing the vortex core. Figure from [4].*

and is proportional to the velocity of the moving vortex, or to the shift of the vortex core position from its equilibrium position. It was found that the z-component of the gyrotropic field, h_z is highly spatially nonuniform, attaining large values near the vortex core but remaining low in areas outside of it. This leads to a significant deformation of the of the $m_z(\mathbf{r}, t)$ magnetization profile of the vortex, creating a 'dip' – a region of opposite polarity close to the moving vortex core – to match the field profile $h_z(\mathbf{r}, t)$ (see Fig. 2.6).

If the gyrofield becomes sufficiently large, the vortex core polarity will completely switch. As mentioned, this gyrotropic field is proportional to the velocity of the moving vortex, leading to the concept of a critical velocity for switching. This notion of a critical velocity is important to this thesis, as it corresponds to a transition from the linear gyrotropic motion to the strongly nonlinear regime of vortex core polarity oscillations. The impact of the existence of these different regimes will be covered in section 4.1.5.

2.2.4 Interaction between vortices

According to condensed matter theory, topological defects – such as vortices – with vorticity $q = \pm 1$ can be considered as positive and negative point charges of unit strength [15], [24]. Letting θ be the angle the unit magnetization vector $\hat{\mathbf{m}}$ makes with a given direction, the angle gradients are associated with components of the electrical field, $(E_x, E_y) = (\partial_y \theta, -\partial_x \theta)$ [24]. Furthermore, the force exerted by a vortex of charge q_1 on another vortex of charge q_2 can be described by,

$$\mathbf{F}_{21} = 2\pi q_1 q_2 \frac{\mathbf{R}_2 - \mathbf{R}_1}{|\mathbf{R}_2 - \mathbf{R}_1|^2} \tag{2.14}$$

where $\mathbf{R}_1$ and $\mathbf{R}_2$ are the positions of the vortices of charge q_1 and q_2 respectively. This force is analogous to the Coulomb force in electrostatics [25]. Thus, for two vortices of charge $q = +1$, Eq. 2.14 predicts a repulsive interaction that increases in strength with decreasing distance between the vortices.

Very little research has been done to investigate this analogy to electrostatics for magnetic vortices. Interactions between two vortices confined in micron-sized thin-film ellipses have been investigated by Hata and Goto [26] and Buchanan *et al.* [27], but neither address the impact of a repulsive force between vortices (Eq. 2.14) on their gyrotropic motion. It should be mentioned that, in [26], the gyration radius were at most 6 nm (in a 1 by 2 µm ellipse), which is not sufficient to observe alterations in trajectory due to vortex interactions.

Buchanan *et al.* [27] notes that "similar to the case of a single vortex in a cylindrical dot, we find that the vortex cores rotate in elliptical orbits around their equilibrium positions". However, no further comment about this elliptical – rather than circular – trajectory is provided.

2.3 Micromagnetic simulations

The energy terms introduced in section 2.1.2 are magnetostatic energy terms. This implies that calculating $\mathbf{M}(\mathbf{r})$ by minimizing the energy 2.7 only holds for systems that are at equilibrium. That is, if $\mathbf{M} \times \mathbf{H}_{\text{eff}} \neq 0$, the system will evolve in time, requiring a dynamic description of the magnetization.

2.3.1 Magnetization dynamics

A dynamic description of the magnetization is given by the Landau-Lifshitz equation. In this approach, the effective field $\mathbf{H}_{\text{eff}}$ is assumed to induce a precession of local magnetization $\mathbf{M}(\mathbf{r}, t)$ of the form:

$$\frac{\partial \mathbf{M}}{\partial t} = -\gamma \mathbf{M} \times \mathbf{H}_{\text{eff}} \tag{2.15}$$

where γ is the gyromagnetic ratio and $\gamma > 0$ determines the precession rate. In addition to this precession term, real magnets are subject to energy relaxation mechanisms, in which the magnetization relaxes towards the direction of the effective field. This can be introduced phenomelogically as a damping term proportional to the component of $\mathbf{H}_{\text{eff}}$ perpendicular to the magnetization, yielding the Landau-Lifshitz equation:

$$\frac{\partial \mathbf{M}}{\partial t} = -\gamma \mathbf{M} \times \mathbf{H}_{\text{eff}} - \frac{\alpha\gamma}{M_S} \mathbf{M} \times (\mathbf{M} \times \mathbf{H}_{\text{eff}}) \tag{2.16}$$

where α is a dimensionless damping constant [28].

2.3.2 Finite difference method

The Landau-Lifshitz equation 2.16 can only be solved analytically for certain rather limited sets of problems [17]. Determining magnetization dynamics with a micromagnetic approach is therefore reliant on numerical solutions.

In micromagnetic simulations, the Landau-Lifshitz equation can be solved by employing the finite difference method. This method is based on a spatial discretization of the problem by subdividing the magnetic object in cells of equal size, each with uniform magnetization. This leads to a discretized version of the micromagnetic free energy and to a corresponding system of ordinary differential equations (ODEs). Using appropriate time-stepping techniques, this system of ODEs is then numerically integrated [28].

In order to accurately model the magnetization dynamics of a ferromagnet by the methods mentioned above, it is important that the magnet is subdivided into an appropriate number of discrete cells. Increasing this number will in general lead to better approximations of the problem. However, an increase in cell number requires more computational power, typically limiting the size of a system that can be simulated for a given number of cells.

Chapter 3

Modeling and methods of analysis

As mentioned in the previous chapter, micromagnetic simulations solve the Landau-Lifshitz equation numerically through methods such as the finite difference method. For a long time the Object Oriented MicroMagnetic Framework (OOMMF), developed by the National Institute of Standards and Technology, has been the primary software for solving micromagnetic problems.

However, OOMMF is CPU-based, which limits the amount of computations that can be performed in parallel. Recent micromagnetic simulation software has seen a change to utilizing the GPU (graphic processing unit) of a computer for its computational power. A CPU consists of a few cores optimized for sequential serial processing while a GPU has a massively parallel architecture consisting of thousands of smaller, more efficient cores designed for handling multiple tasks simultaneously [29]. As a micromagnetic simulation typically involves solving the Landau-Lifshitz equation for each cell in the grid as it evolves through time, an increased number of cores means that the magnetization moment of an increased number of cells can be calculated simultaneously.

One such a GPU-accelerated micromagnetic simulation program is MuMax3, developed at the DyNaMat group (Dynamics of Functional Nano Materials) at Ghent University.

3.1 Introduction to MuMax3

MuMax3 was used for all the simulations in this thesis, as its high performance and low memory requirements allow for large-scale simulations to be performed in limited time and on inexpensive hardware [30]. Furthermore, MuMax3 provides a dedicated scripting language, which makes it simple to define fairly complex simulations.

3.1.1 Modeling a system

The type of system to be modeled is defined by a wide range of parameters. For the purpose of the simulations performed in this thesis the relevant parameters are: Exchange stiffness A, saturation magnetization M_s, anisotropy constants K_u or K_c, and anisotropy directions.

Depending on whether the system has a uniaxial or cubic anisotropy, one or two directions are specified, respectively. In the case of cubic anisotropy, the third easy axis is calculated as the cross product of the first two directions [30]. For uniaxial anisotropies, K_u should be specified, for cubic K_c. Anisotropy axes are easy axes if $K > 1$, and hard if $K < 0$.

The geometry of the material can be specified as primitive shapes such as a circle, a rectangle, an ellipse or a cylinder. Translating or rotating the shapes is trivial, as is adding several shapes to create more complex structures. Alternatively any other shape can be defined by importing a 2-color image file. In any case, the grid and cell size must be defined. Regarding the former, the only important thing to consider is that there are enough grid cells to contain the given geometry when dividing it into cells of the given cell size. A proper choice of cell size is one that is smaller than the exchange length l_{ex} (Eg. 2.9).

For ferromagnetic materials, the exchange length is typically 5-10 nm [22]. However, as the material to be modeled needs to be an integral multiple of the cells in both x- and y-directions, the cell size may deviate from l_{ex}. Furthermore, the values of A, M_s, and K need to be chosen so as to describe the material correctly in relation to experimental results, and l_{ex} will vary accordingly.

3.1.2 Running a simulation

MuMax3 offers a few different options for running a simulation. A brief introduction to these will be given, with focus on the ones relevant to this thesis.

The standard method of running a simulation of a dynamic evolution of the magnetization is evoked by the native function `run(time)`. This function runs the simulation for the time given, using sensible error settings. Optionally, a different solver may be chosen, as a number of explicit Runge-Kutta methods for advancing the Landau-Lifshitz equation (Eq. 2.16) are provided. The default solver for dynamical simulations is RK45, which employs the Dormand-Prince method.

When relaxing the magnetization state of a system to equilibrium, typically the `relax()` function is used. This function assumes all excitations to be off (e.g., temperature, electrical current, time-dependent magnetic fields). Furthermore, it disables the precession term Eq. 2.16, which decreases the simulation time required to calculate the energy minimum of the system.

Other functions include `minimize()` and `runwhile(condition)`. The former closely resembles the `relax()` function, but employs a different method in order to minimize the total energy. `runwhile(func() bool)` runs a simulation as long as an arbitrary condition is met, for example the average magnetization being below a certain value.

3.1.3 Data output

MuMax3 provides several options for recording the data of a simulation, for example: A data table, containing by default the time and average (normalized) magnetization in x-,y-, and z-directions. Several other quantities, such as the effective field $\mathbf{H}_{\text{eff}}$ or any of the energy terms in Eq. 2.7, can be added as columns to this table, and will then be stored as spatial averages. All space-dependent quantities, such as $\mathbf{m}(\mathbf{r})$, can be output and saved as individual vector fields in a "OVF" (OOMMF Vector Field) data format. How often output should be saved, either to the data table or as a separate OVF file, can be defined.

Furthermore, user-defined output can be freely generated. For example a TXT file storing all parameters. It is also possible to take snapshots of the magnetization, generating JPG files directly, or to utilize the mumax3-convert option to generate images from OVF files.

An OVF file can be displayed as a vector field, as shown in figure 3.1. As can be seen from this figure, areas with uniform color indicates that all the moments in the area are aligned parallel to one another. A single-domain structure will thus appear as a single, uniform color — red if it is magnetized in the positive x-direction, cyan if it is is magnetized in the negative x-direction, and so on. This color scheme is the standard in MuMax3.

In principal, any color can be chosen to indicate magnetization direction. For comparison with experimental results, a black-gray-white scheme is commonly chosen, as this is how the magnetization will appear when probed with imaging techniques such as X-ray photoemission electron microscopy (X-PEEM) or magnetic force microscopy (MFM). However, this makes it more difficult to differentiate the magnetization directions in a multidomain state, as areas magnetized in both negative and positive y-direction will have the same shade of grey.

3.2 Modeling the structures

A brief introduction to modeling in MuMax3 has been given. More detail into how the material system of interest was defined will be outlined in this section.

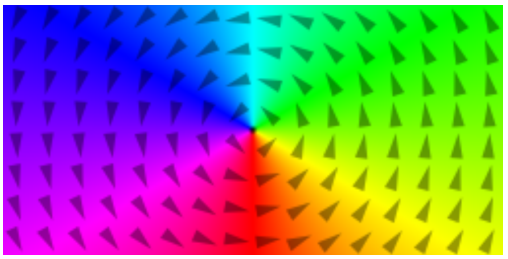

FIGURE 3.1: *Vector field output from MuMax3 simulation.*

3.2.1 Model system

The simulations were all set up with the same basic parameters describing the material. The values for the exchange stiffness $A = 1.7 \times 10^{-12}\,\mathrm{J/m}$, saturation magnetization $M_s = 2.75 \times 10^5\,\mathrm{A/m}$, and anisotropy constant $K_{c1} = 1600\,\mathrm{J/m^3}$ were chosen after Slöetjes [31], with small alterations. These values were obtained by a systematic approach, varying each parameter individually in order to define a set giving the best correspondence between simulations and experimental measurements of the magnetization of LSMO-microstructures with dimensions $L \times 2\,\mu\mathrm{m}$ (where L was varied to observe for which values the islands obtained a single-domain magnetization) by Folven *et al.*

By these values, the exchange length was calculated according to equation 2.9, giving a value of 5.98 nm and making 5 nm a good choice for the cell size. The thickness of the film was set to 35 nm. This is the typical thickness LSMO films are grown to experimentally, by the research group for which the work in this thesis was performed. As evident from the expression for the eigenfrequency of the vortex translational mode Eq. 2.13, the aspect ratio between radius and thickness is of importance. This has also been investigated in several papers [32], [33], [34]. Therefore, we expect the eigenfrequency to vary accordingly as we vary the disk diameter. However, the impact of varying this ratio will not be investigated in this thesis. Rather, we are aware that any change in diameter and resulting change in eigenfrequency is not a result of the different radius explicitly, but rather a result of a difference in aspect ratio. As such, for the structures investigated in this thesis, they all have a thickness of 35 nm.

The anisotropy was defined as cubic, with the first two axes being the x- and y-axis respectively. MuMax3 calculates the third axis as a cross product of these, but by virtue of the limited thickness this anisotropy direction is greatly repressed.

3.2.2 Initial magnetization

As stated in section 2.2.1, the magnetic vortex is the ground state in magnetic structures with certain geometrical and material parameters. However, as the aim of this thesis

was not to investigate the natural occurence of vortices, but rather their dynamic behavior, all structures where initialized to appropriate vortex states by utilizing MuMax3 functionality.

For a single disk, defining a vortex state is trivial, and in fact also a native function in MuMax3. In overlapping geometries, it is a bit more complicated, and requires a few translational operations to produce the desired structures. This is illustrated by the code excerpts in Listing 3.1 and 3.2.

```
//Defining the geometry of the structure as a circle with diameter of 2e-6 m

diameter := 2e-6
setgeom(circle(diameter))

//Defining the magnetization of the structure. The input parameters for the
//function vortex(c, p) are the chirality and the polarity of the vortex.

m = vortex(1, 1)
```

LISTING 3.1: *Code for generating the vortex magnetization state in a circular disk*

```
//Defining the geometry of the structure as two circles with diameters of 1e-6 m
//and a distance of 0.4e-6 m between the circle centers

diameter := 1e-6
centerDist := 0.4e-6

//MuMax3 defines the center of the mesh as the position (0, 0), thus each circle
//should be moved a distance of centerDist/2 in the x-direction to either side of
//the origin

translDist := centerDist/2

//The geometry and position of each circle is defined separately, adding them to
//each other when defining geometry (setgeom)

a := circle(diameter).transl(-translDist, 0, 0)
b := circle(diameter).transl(translDist, 0, 0)
setgeom(a.add(b))

//Defining regions in order to be able to define the magnetization of each
//circle separately

defregion(1, xrange(-inf, 0)) //left half
defregion(2, xrange(0, inf))  //right half

//Defining the magnetization of each region/circle

m.setRegion(1, vortex(-1, 1).transl(-translDist, 0, 0))
m.setRegion(2, vortex(1, 1).transl(translDist, 0, 0))
```

LISTING 3.2: *Code for generating the two vortex magnetization state in two overlapping circular disk*

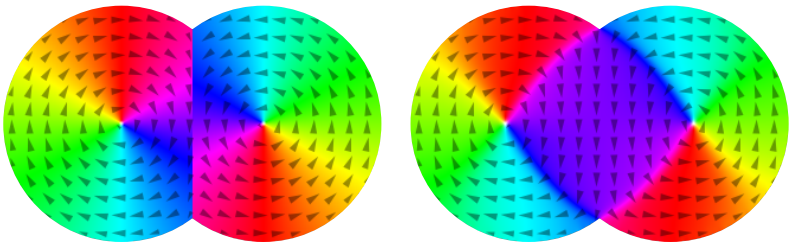

(a) (b)

FIGURE 3.2: *(a) Magnetization state as initialized by MuMax3 and (b) initial magnetization upon letting the state in (a) relax to equilibrium.*

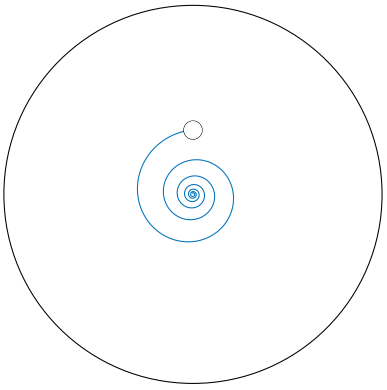

FIGURE 3.3: *Illustration of the spiraling motion of the vortex translational mode.*

The code in Listing 3.2 will generate the magnetization state seen in figure 3.2(a), which will relax to the equilibrium state seen in figure 3.2(b). As this relaxation step requires a fair amount of computation time, the equilibrium state was stored as an OVF file, subsequently importing it for all simulations of same geometry and core polarities.

3.2.3 Vortex gyration

The vortex translational mode was provoked by displacing the vortex from its equilibrium position using an external static in-plane magnetic field in the order of a few mT. Such a field serves to increase the area magnetized parallel to the field direction, thus pushing the vortex out of its equilibrium position. The system was then allowed to relax in this field by employing the native `relax()` function in MuMax3 (see Sec. 3.1.2). Upon removing the field, the simulation was continued using the `run(time)` function, allowing the vortex core to relax dynamically back to its equilibrium position following the characteristic spiral motion (see Fig. 3.3).

The radius of the resulting gyrotropic motion is determined by the strength of the applied field, as a stronger field will correspond to a larger displacement of the vortex core.

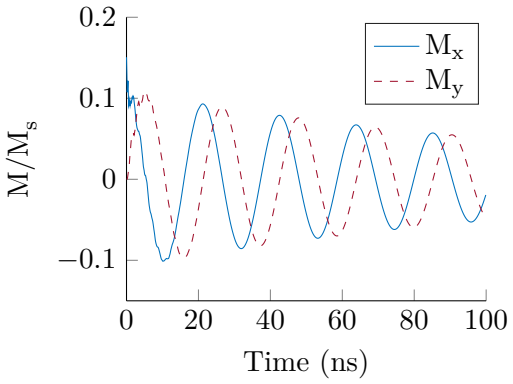

FIGURE 3.4: *Time evolution of average magnetization in a circular LSMO disk, after initial displacement of vortex core by a static in-plane magnetic field.*

3.3 Analysis of output data

The relevant data to be analysed for each simulation, as well as the method of analysis will be given in this section.

3.3.1 Temporal oscillation of the magnetization

The time evolution of the magnetization can be visualized by plotting the magnetization in a given direction over time. An example of such a plot can be seen in figure 3.4, in which the damped oscillation, caused by the spiral motion of the vortex core towards its equilibrium position, can observed. Notice that the $\langle M_x \rangle$ and $\langle M_y \rangle$ components oscillate in harmony. This is to be expected from the symmetric motion of the gyration around the equilibrium position.

3.3.2 Eigenfrequency of the vortex motion

The eigenfrequency of the vortex translational mode (as described in section 2.2.3) can be extracted through a Fourier transform of the time evolution of $\langle M_x \rangle$ [11], [27]. This was done using the Fast Fourier Transform (FFT) in MATLAB, a computational method that optimizes the calculation of the discrete Fourier transform (DFT). The method for extracting the eigenfrequencies will be explained here, and the full code can be found in appendix A.1.

The FFT allows us to efficiently estimate component frequencies in data from a discrete set of time-based data sampled at a fixed rate. The component frequencies are defined by:

$$Y(k) = \sum_{j=1}^{n} X(j) W_n^{(j-1)(k-1)} \tag{3.1}$$

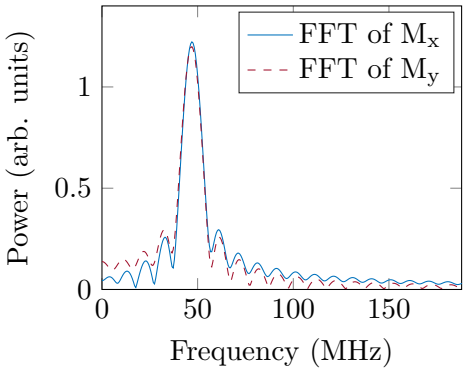

FIGURE 3.5: *Frequency spectrum of the gyrating vortex core motion.*

where $Y(k)$ and $X(j)$ are the components of the vectors $\mathbf{Y}$ and $\mathbf{X}$, containing the time domain and frequency domain data respectively. $W_n = e^{(-2\pi i)/n}$ is the nth root of unity.

Calculating $\mathbf{Y}$ by the native FFT function `Y = fft(X, n)` returns the n-point DFT of $\mathbf{X}$. If no value is specified for n, $\mathbf{Y}$ will have the same length as $\mathbf{X}$. The execution time for of the FFT depends on the length of the transform. However, this time is greatly reduced for lengths corresponding to powers of two [35]. For values of n less than the length of $\mathbf{X}$, only the first n elements of $\mathbf{X}$ are used to compute the transform. Therefore, it is common to define n as the next power of two from the length of $\mathbf{X}$, which effectively means padding the $\mathbf{X}$ with trailing zeros. This will also reduce the frequency spacing between the components of $\mathbf{Y}$. It should be noted that this will not increase the frequency resolution, as this is dependent on the sampling frequency of the time-based data. Rather, it will result in interpolated plot points between the different frequency components. However, if there is little noise present in the $\mathbf{X}$-data, this interpolation will typically be quite accurate.

To visualize the DFT, it is common to plot the amplitude of $\mathbf{Y}$. In our case, such a plot will be symmetric about its midpoint, due to the fact that the Fourier transform for real values is conjugate symmetric, i.e., $Y(-k) = Y^*(k)$. Because of this the second half of the DFT is unimportant to our results. Furthermore, as we are interested in the eigenfrequency, and not any spectral power value, the units of the amplitude of $\mathbf{Y}$ are considered arbitrary. An example of the output from an FFT can be seen in figure 3.5.

3.3.3 Vortex core trajectories

A simple method for investigating the predicted repulsive interaction between vortices, is to observe the trajectories of the vortex cores as they gyrate about their respective equilibrium positions. However, tracking the cores by analyzing the output data provided by MuMax3 is not straight forward, and the method for doing so will therefore be described.

The easiest way of locating a vortex is to locate the position where $\mathbf{M}_z$ has its maximum (for $p = +1$) or minimum (for $p = -1$) value. As the output stored in the data table (see Sec. 3.1.3) are spatial averages of the magnetizations, $\langle M_x \rangle$, $\langle M_y \rangle$, and $\langle M_z \rangle$, this data cannot be used to locate or track core position. The other option is to store the magnetization distribution $\mathbf{M}(\mathbf{r})$ at specific times as separate vector fields (OVF files). This makes it possible to locate the core position by the approach mentioned above. Locating the core position individually for each stored vector field, and then plotting this as a function of time will yield the desired vortex core trajectory.

The approach outlined above works well in the case of one vortex. It is also sufficient for locating two vortices with opposite polarities, as this would simply involve locating both the maximum and minimum of $\mathbf{M}_z$, instead of just one of them. However, for two vortices of equal polarity a few issues may arise:

- If tracking the cores by locating the first and second highest (or lowest) values of $\mathbf{M}_z$, there is no guarantee that the highest value will always correspond to one vortex and the second highest to the other.
- There is a possibility of the vortex core occupying more than one cell in the grid mapping the magnetization distribution. If the center of the core is located close to the border between two cells, we can expect the magnitude of $\mathbf{M}_z$ for both cells to be close to a maximum (or minimum) value. This leads to a problem similar to the one described in (1). The diameter of the vortex core is approximately equal to the exchange length Eq. 2.9 [3]. As the cell size is set to a value below this, the possibility of two neighboring cells having extreme values of $\mathbf{M}_z$ increases.

The solution to these issues will be outlined here, the full code can be found in the appendix A.2. First, the absolute value of M_z was taken, in order to account for both positive and negative polarities. Then, the column of the grid (corresponding to a given x-value) containing the maximum value was located using native MATLAB functions. After locating at the row in this column containing the maximum value, the column and the ones to either side of it was filled with elements of zero. The process can then be repeated for any given number of vortex cores.

Chapter 4

Results and Discussion

4.1 Single vortex dynamics

Initial simulations focused on investigating the rotation of a vortex core around its equilibrium position, as well as the influence of varying material parameters on the frequency spectra. A single circular disk with a diameter of 2 µm was initialized in the characteristic vortex state (fig 4.1) with a polarity of $p = +1$, and allowed to relax in order to verify the stability of this state. The material parameters were chosen as described in section 3.2.1, that is, $M_s = 2.75 \times 10^5\,\mathrm{A/m}$, $A = 1.7 \times 10^{-12}\,\mathrm{J/m}$, and $K = 1600\,\mathrm{J/m^3}$.

4.1.1 Gyrating motion

Following the approach illustrated in [27], simulations of the gyrating motion dynamics were carried out by shifting the vortex from its initially centered vortex state using a static in-plane magnetic field of $H_x = 1\,\mathrm{mT}$, and a large damping parameter ($\alpha = 1.0$). The magnetization state was allowed to relax, before removing the field and continuing

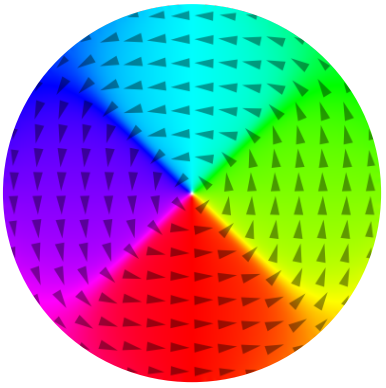

FIGURE 4.1: *Initial magnetic vortex state in a single 2 µm LSMO disk. The white core indicates* $p = +1$.

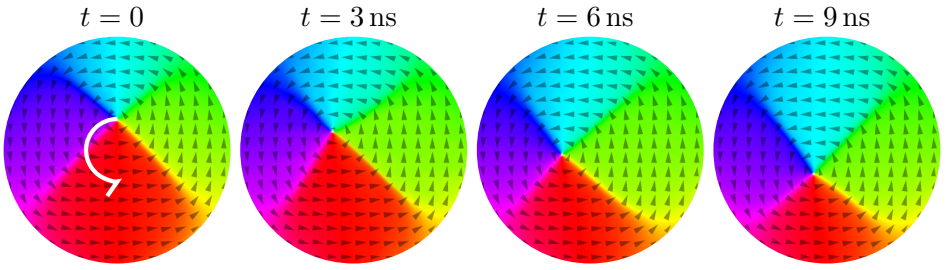

FIGURE 4.2: *Gyrating motion of the vortex core in a single 2 µm LSMO disk. The white core indicates* $p = +1$.

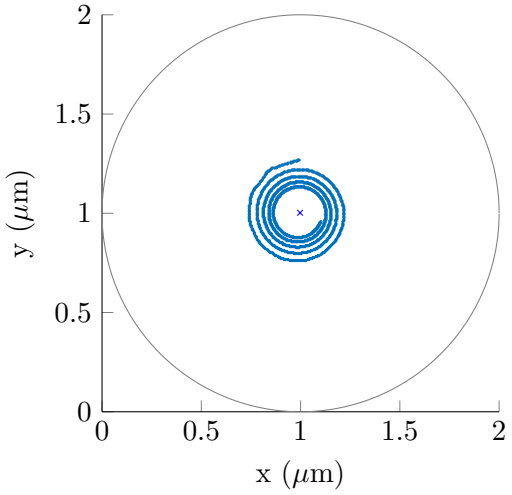

FIGURE 4.3: *Vortex core trajectories in a single 2 µm LSMO disk.*

the simulation using a smaller damping parameter ($\alpha = 0.005$). This latter value of α differs slightly from the one used in [27], and was chosen as it provides enough damping to be able to produce a discernible spiraling direction, while at the same time making it possible to accurately observe the shape of the trajectory.

An illustration of the gyration motion can be seen in figure 4.2, while a plot of the vortex trajectory can be seen in figure 4.3. Note the direction of the gyrating motion, which is counter-clockwise, in correspondence with the theory (Sec. 2.2.3).

It should be mentioned that the simulation times used were not sufficient for the vortex core to relax back to its equilibrium position. However, for the purpose of extracting the eigenfrequency and analysis of the trajectory shape, this is insignificant as long as the number of full circulations around the equilibrium position is sufficient.

The eigenfrequency of the gyrating motion was calculated by the approach described in section 3.3.2. The oscillations of $\langle M_x \rangle$ and $\langle M_y \rangle$ can be seen in figure 4.4(a), and the corresponding Fourier spectrum in figure 4.4(b).

The eigenfrequency was found to be 47 MHz, which is in agreement with other findings. In experiments, Novosad *et al.* [11] measured an eigenfrequency of 83 MHz for

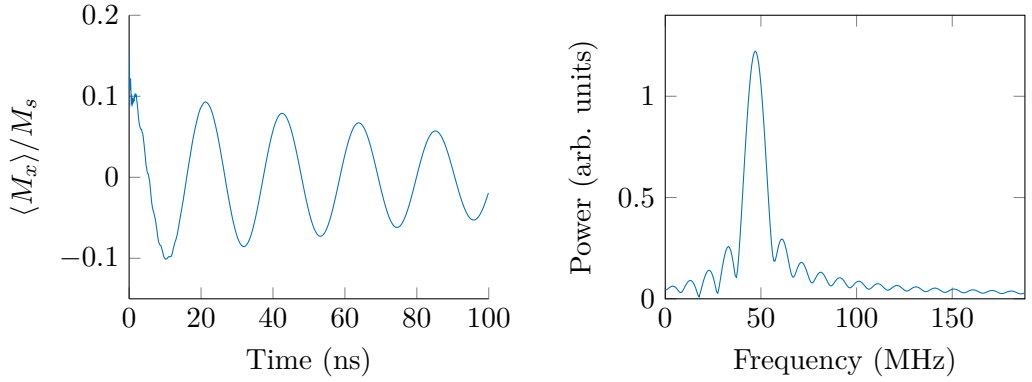

(a) (b)

FIGURE 4.4: *(a) Time evolution of average magnetization in a circular LSMO disk with $d = 2\,\mu$m, after initial displacement of vortex core by a magnetic field of $H_x = 1\,$mT. (b) Frequency spectrum of the gyrating vortex core motion. The frequency peak is located at 47 MHz.*

a circular Permalloy disk with a diameter of 2 µm and a thickness of 20 nm. Increasing the thickness of the sample, Eq. 4.1 predicts an increase in frequency. This is the same expression for the eigenfrequency introduced in section 2.2.3, included here for ease of reference.

$$\omega_0(\beta, R) = 2\gamma M_s \left[4\pi F_v(\beta) - \frac{1}{2}\left(\frac{l_{ex}}{R}\right)^2 \right] \tag{4.1}$$

Based on this notion, we would expect our structures, which have a thickness of 35 nm to have a higher eigenfrequency. However, Eq. 4.1 also predicts that an increase saturation magnetization will correspondingly increase the frequency. As the saturation magnetization in [11] was 7.5×10^5 A/m, it is reasonable that LSMO – which has a significantly lower saturation magnetization – also exhibits a lower eigenfrequency of the gyrotropic motion. In fact, calculating the eigenfrequency of the structure in [11] by Eq. 4.1, changing the saturation magnetization and the exchange stiffness to fit the values for LSMO, we obtain a frequency of 30 MHz.

It has been established that the vortex gyrotropic mode has a rather low eigenfrequency, < 1 GHz, for dots with thicknesses much smaller than the diameter [3]. A complete analytical derivation of the eigenfrequency is beyond the scope of this thesis.

In the case of a polarity of $p = -1$, the eigenfrequency was found to be the same, the only difference being the direction of rotation, as expected from theory.

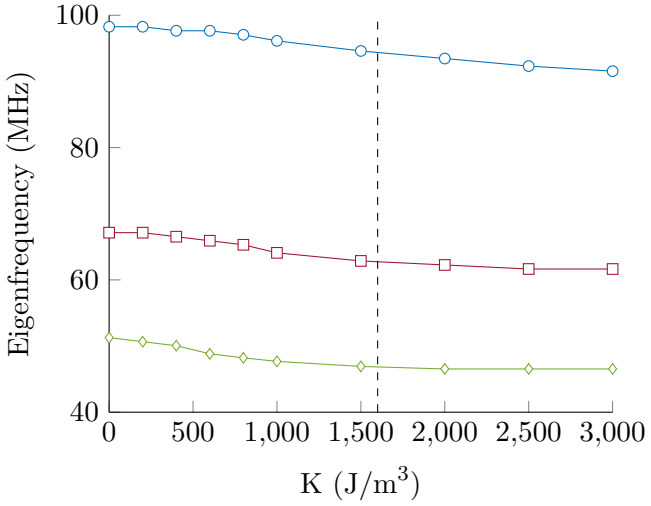

FIGURE 4.5: *Translation mode eigenfrequency versus the anisotropy constant K for cylindrical dots with diameters $d = 1\,\mu m$ (blue line), $d = 1.5\,\mu m$ (red line), and $d = 2\,\mu m$ (green line). The dashed line indicates the typical value of K used for modeling LSMO.*

4.1.2 Effect of varying the anisotropy constant

LSMO differs from many other metallic ferromagnets in that is has a high magnetocrystalline anisotropy. As previous research into magnetic vortices has focused primarily on materials such as permalloy, in which the magnetocrystalline anisotropy is negligible [27], simulations investigating the impact of varying K was performed.

The calculated eigenfrequencies for different values of K are shown in figure 4.5. From [32], [33], [34] we know that the eigenfrequency varies significantly with the aspect ratio between the thickness and lateral dimensions of the film. As such, simulations were also performed varying the value of K for disks with diameters of 2 µm, 1.5 µm and 1 µm, in order to observe the relative impact of K on the eigenfrequency as compared to impact of the aspect ratio. In these simulations, a field of 2.5 mT was used to displace the vortex core.

As can be seen from figure 4.5, the impact of varying K does not have a large impact on the eigenfrequency, especially compared to the difference observed when varying the disk diameter. However, the fact that there is a slight change, suggests that the analytical approach is not adequate for materials in which the mangetocrystalline anisotropy is more protrudent than it is in for example permalloy. Further investigation can be done into this matter, but will not be covered in this thesis. The variance is hardly more than a few MHz, around 10 MHz at most. Further simulations will use the standard value of $1600\,J/m^3$, as described in section 3.2.1.

Another interesting aspect is how varying the anisotropy contant alters the configuration of the initial magnetization state. This can be seen in figure 4.6. Here, for

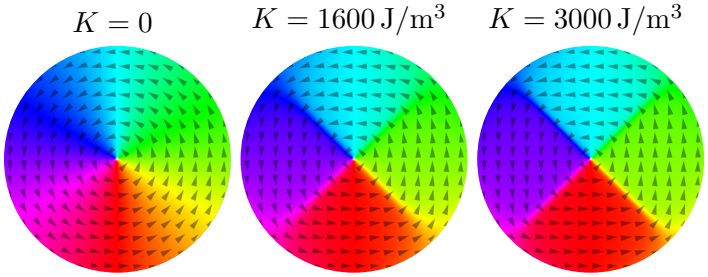

FIGURE 4.6: *Vortex magnetization state in a single 2 µm LSMO disk for different values of the anisotropy constant.*

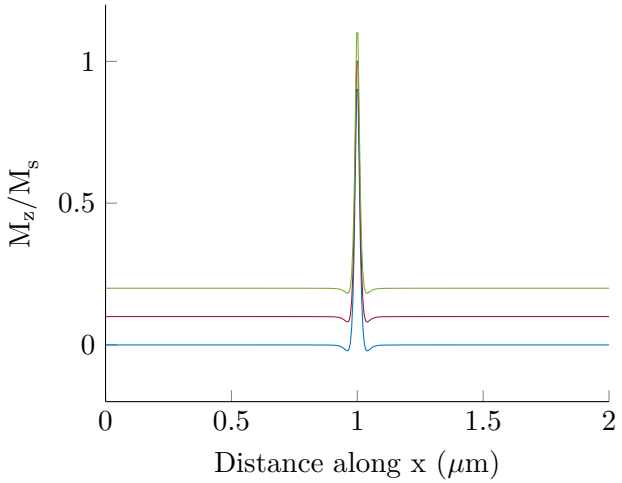

FIGURE 4.7: *Vortex core magnetization profile for $K = 0$ (blue line), $K = 1600\,\mathrm{J/m^3}$ (red line), and $K = 3000\,\mathrm{J/m^3}$ (green line). The latter two profiles are shifted vertically by 0.1 and 0.2 for clarity.*

increased values of K a smooth transition of the in-plane magnetization direction is abandoned in favor of sharp walls between domains magnetized along either of the easy directions. As the anisotropy constant is a measure of how strongly the magnetic spins prefer to align along the easy axes, this is to be expected. Note, however, that the size of the vortex core does not change. This can be seen in figure 4.7, where the vortex core magnetization profile is illustrated by a plot of M_z along a line parallel to the x-axis through the vortex center.

4.1.3 Effect of varying the saturation magnetization

Simulations were performed with varying saturation magnetization. The resulting eigenfrequencies can be seen in figure 4.8. As for the simulations with varying K, a field of 2.5 mT was used to displace the vortex core. These results corresponds well with the analytical expression (Eq. 4.1). By rearrangement and inserting the full expression for the exchange length $l_{ex} = \sqrt{\frac{2A}{\mu_0 M_s}}$, we get:

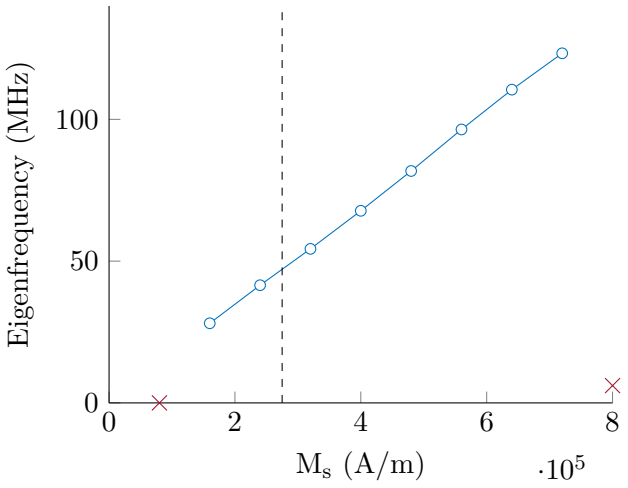

FIGURE 4.8: *Translation mode eigenfrequency versus the saturation magnetization M_s for circular disks with diameters $d = 2\,\mu$m. The dashed line indicates the typical value of M_s used for modeling LSMO.*

$$\begin{aligned}\omega_0(\beta, R) &= 2\gamma M_s\left[4\pi F_v(\beta) - \frac{1}{2}\left(\frac{l_{ex}}{R}\right)^2\right] \\ &= 8\gamma M_s \pi F_v(\beta) - \frac{2\gamma M_s}{R^2}\frac{2A}{\mu_0 M_s^2} \\ &= 8\gamma\pi F_v(\beta) M_s - \frac{4\gamma A}{R^2\mu_0}\frac{1}{M_s}\end{aligned} \tag{4.2}$$

If all other factors are kept constant, we see from this expression that the eigenfrequency ω_0 varies with the saturation magnetization M_s according to $\sim M_s - \frac{1}{M_s}$. For values of M_s higher than one, this is a near linear function, corresponding well with the results. However, looking at 4.8 we see that for two values of M_s (indicated by red crosses) the eigenfrequencies does not follow this linearity. The explanation for this is as follows. For $M_s = 8 \times 10^4$ A/m, the field of 2.5 mT is sufficient to magnetize the disk to a monodomain state. That is, the magnetic field drives the vortex core "out" of the structure completely. In the case of $M_s = 8 \times 10^5$ A/m, the magnetic field is not sufficient to push the vortex core out of its equilibrium state by any significant measure, restricting any gyrating motion. Both of these can easily be verified by looking at the respective plots for the time evolution of the magnetization (fig. 4.9).

The initial magnetization states can be seen in figure 4.10. Two things should be noticed. First, the same increase in sharpness of the domain walls observed for increasing values of K, can be seen here for lower values of M_s. The reason for this is that for lower values of M_s, the contribution from the anisotropy constant becomes greater, favoring alignment along the easy axes (the x- and y-directions). Second is the variation in diameter of the vortex core, as illustrated in figure 4.11. This is to be expected when we consider that the diameter of the core is approximately the same as the exchange

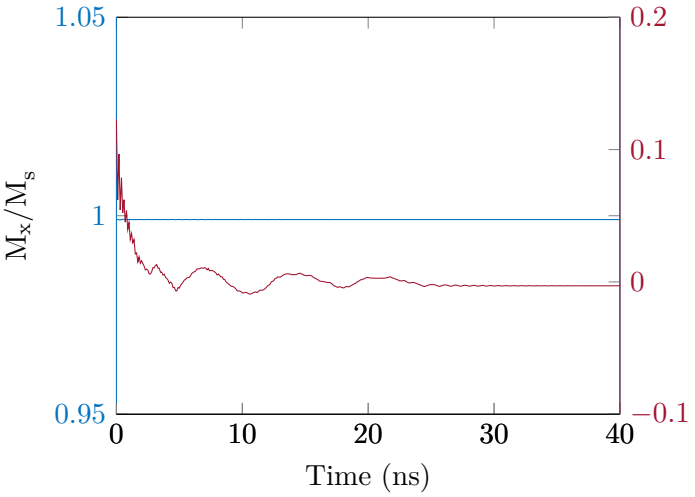

FIGURE 4.9: *Time evolution of average magnetization* $\langle M_x \rangle$ *for* $M_s = 8 \times 10^4$ A/m *(blue line), and* $M_s = 8 \times 10^5$ A/m *(red line).*

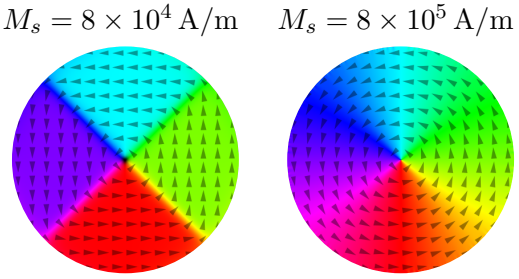

FIGURE 4.10: *Vortex magnetization state in a single 2 µm LSMO disk for different values of the saturation magnetization.*

length $l_{ex} = \sqrt{\frac{2A}{\mu_0 M_s^2}}$. It is simple to see from this expression that an increase in M_s will decrease the vortex core diameter.

4.1.4 Effect of varying the exchange stiffness

As with the saturation magnetization, the exchange stiffness A also appears in the analytical expression for the eigenfrequency (see Eq. 4.2). Simulations were done investigating the effect of varying A on the eigenfrequency of the gyrotropic motion in a 2 µm disk. Again the displacement field was set to 2.5 mT, similar to the simulations investigating the effect of varying K and M_s. The values of K and M_s were set to K = 1600 J/m^3 and 2.75×10^5 A/m respectively, the standard values used in this thesis.

The result can be seen in figure 4.12. The idea was to vary the value of A two orders of magnitude around the typical value used for modeling LSMO.

Compared to the results in figure 4.8, the results in figure 4.12 suggest that the eigenfrequencies do not vary with A in the way that was expected. Again, looking at the analytical expression (Eq. 4.2, we expect it to vary linearly with A. It can be argued

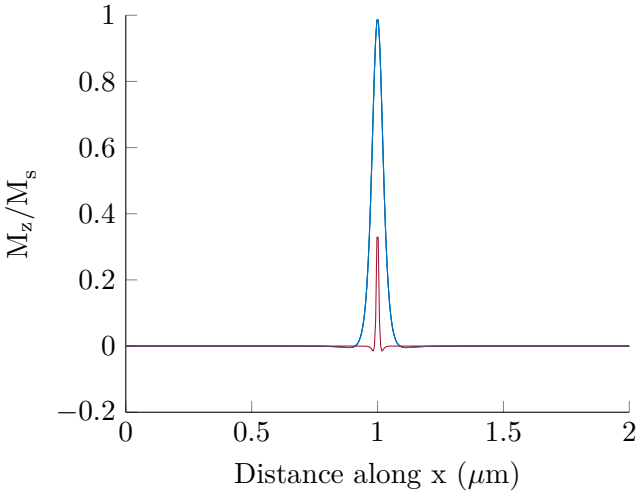

FIGURE 4.11: *Vortex core magnetization profile for* $M_s = 8 \times 10^4$ A/m *(blue line) and* $M_s = 8 \times 10^5$ A/m *(red line).*

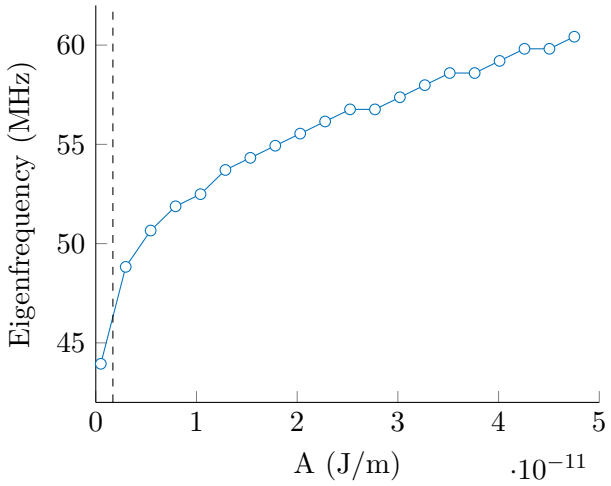

FIGURE 4.12: *Translation mode eigenfrequency versus the exchange stiffness A for circular disks with diameters d = 2 µm. The dashed line indicates the typical value of A used for modeling LSMO.*

that above 1×10^{-11} J/m, the behavior is close to linear, with any deviance being due to a limited resolution caused by the fixed cell size. However, for the lower values of A, the linear relationship is abandoned.

A possible explanation for this is that the cell size is insufficient. As mentioned in section 3.1.1, a good choice of cell size is considered to be one that reflects the exchange length l_{ex}. For too low values of A, it therefore means that the chosen cell might not adequately model the system. In order to verify this hypothesis, a few simulations were performed with cell size exactly equal to the exchange length. Only a few values of A were used, however, as a decrease in cell size will significantly increase the simulation time required.

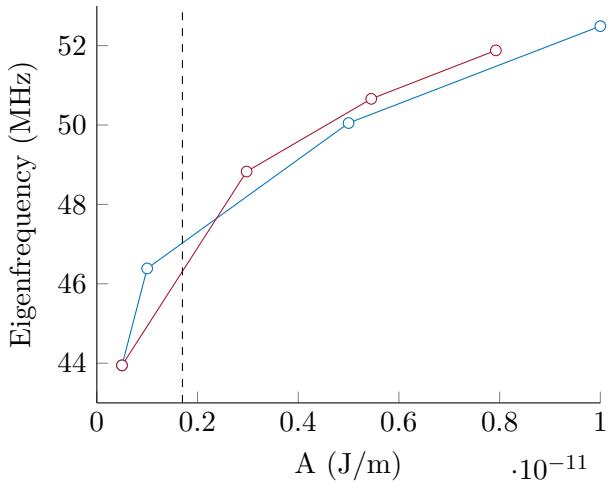

FIGURE 4.13: *Translation mode eigenfrequency versus the exchange stiffness A for circular disks with diameters $d = 2\,\mu$m, with cell size equal to exchange length (blue line), and with a constant cell size of 5 nm (red line). The dashed line indicates the typical value of A used for modeling LSMO.*

Looking at the results in figure 4.13, it seems possible that a poor choice of cell size is partially responsible for the deviation from the expected linear behavior. However, for the smallest values of A, the eigenfrequency decreases drastically abandoning any linear relation with A. A comprehensive investigation into this matter will not be presented, but a possible explanation might be as follows: As the decrease in cell size required to simulate the structure for the lowest value of A accurately will come at a considerable cost of computational speed, the running time of the simulation was reduced. As a result, the already low eigenfrequency might not have allowed for sufficient oscillations around the equilibrium position, to be able to accurately calculate the eigenfrequency.

The initial magnetization states are shown, for two extreme values of the exchange stiffness, in figure 4.14. The sharp domain walls for the low, as compared to the high, value of A, is due to the fact that a higher exchange stiffness will force neighboring spins to align with one another, creating a smoother transition of the magnetization, as the energy gain of domain wall creation is insufficient. Again, an argument can be made for the domain walls being a result of the high anisotropy constant.

Another aspect is the enlarged vortex core for higher values of A, illustrated by the vortex core magnetization profile in figure 4.15. The same explanation can be given here, as for the case of low M_s: The core diameter correlates to the exchange length, and this increases with A.

4.1.5 Linear and nonlinear regimes

Another aspect that should be addressed, before moving beyond the system of a single disk, is what we will refer to as the linear and nonlinear regimes. The full theory behind

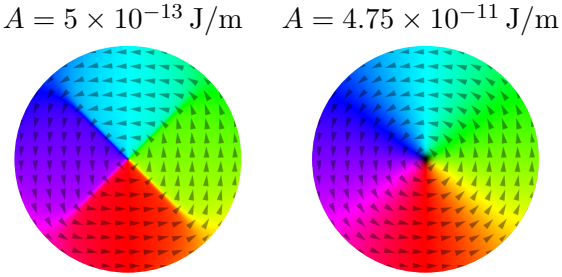

FIGURE 4.14: *Vortex magnetization state in a single 2 µm LSMO disk for different values of the exchange stiffness.*

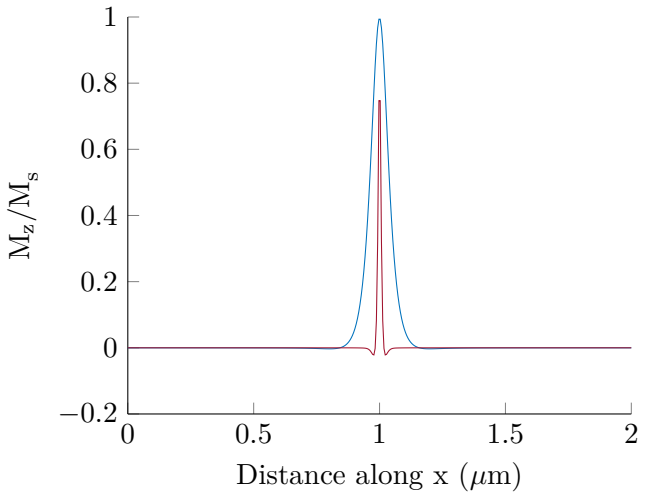

FIGURE 4.15: *Vortex core magnetization profile for* $A = 4.75 \times 10^{-11}$ J/m *(blue line) and* $A = 5 \times 10^{-13}$ J/m *(red line).*

this behavior is complex, and will only be covered briefly in this thesis, as a full quantum mechanical investigation is beyond its scope.

As explained, the gyrating motion of the vortex can be provoked by applying a static in-plane magnetic field, and then removing it abruptly. However, if this magnetic field exceeds a certain value, a switch of the vortex polarity can be observed. Spin waves are emitted in this event. This polarity switching occurs when the vortex core reaches a certain threshold velocity, as explained in section 2.2.3.

Although this magnetization switching has many promising applications within e.g. nonvolatile magnetic memories [26], for the purpose of studying the electrostatic-like behavior of two interacting vortices, this spin-wave emission causes undesirable disturbances. As can be seen in figure 4.16, although a higher field will cause an initial displacement further from the equilibrium position, the following core polarity switching "pushes" the core back, resulting in a trajectory with smaller radius. Furthermore, the switching might occur an odd number of times, resulting in a different polarity than initially defined.

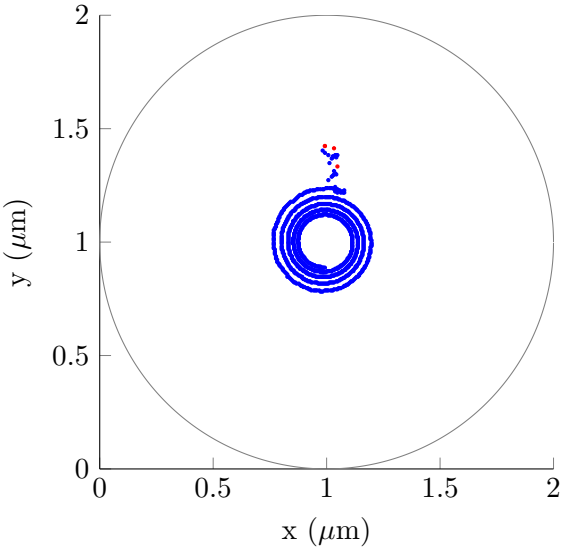

FIGURE 4.16: *Vortex core trajectories in a single 2 µm LSMO disk. Core polarity is indicated by blue ($p = +1$) and red ($p = -1$).*

We will refer to the case where no switching occurs as the linear regime, and, consequently, the case where switching does occur as the nonlinear regime.

4.2 Coupled vortices

Although extensive research has been done focusing on single vortices, two vortices confined in an ellipse, and the magnetostatic interaction between vortices in laterally separated disks, little investigations have been done on the interaction between two vortices, with regard to the electrostatics analogy described in section 2.2.4.

A simple way of investigating this phenomenon, is to observe the vortex trajectories, and how they differ by vortex-vortex interaction when varying parameters such as the center-to-center distance between the disks, and the rotational direction of the cores. The latter is, as previously mentioned, solely determined by the core polarity, and will – coupled with the direction of the displacement field – determine how close the cores get when following the circular trajectory around their equilibrium positions. This will be explained further in section 4.2.1.

Two overlapping disks, rather than an ellipse, were chosen as the geometry in which to study the interaction between two vortices. The reason behind this mainly that it allows for easy expansion of the system into a linear or two dimensional array.

The diameter of each individual disk was set to 1 µm, as compared to a diameter of in 2 µm for the case of a single disk, in order to maintain reasonable simulation times.

A total of four different systems were investigated. All with two overlapping disks, but with different center-to-center distance and both equal and opposite polarities. The center-to-center distances chosen were 0.4 and 0.6 µm. We will refer to the polarity of the left vortex as p_1, and that of the right vortex as p_2.

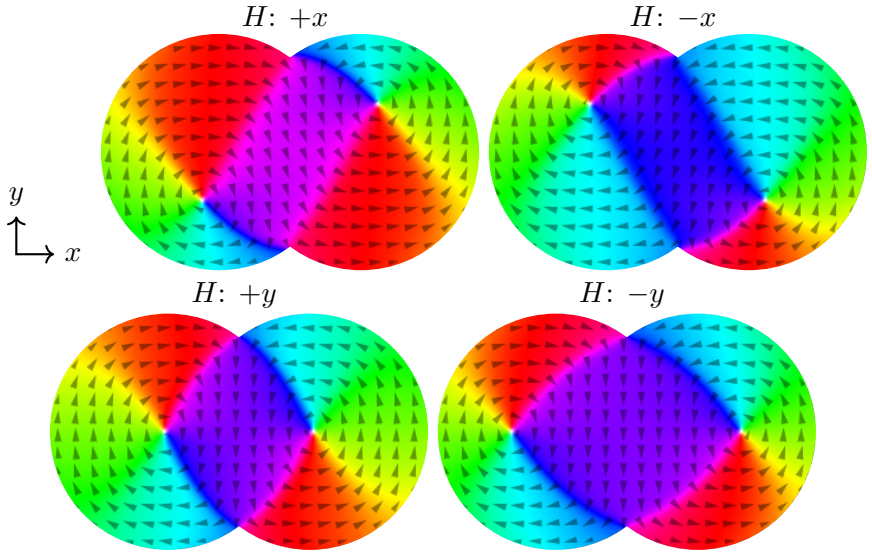

FIGURE 4.17: *Magnetic vortex states in two overlapping LSMO disks after an applied magnetic field H in the direction indicated.*

4.2.1 Modes of gyration

Different from the situation with a single disk, in a system of two vortices in two overlapping disks, the direction of the applied magnetic field is of importance, as the system is no longer directionally isotropic. Furthermore, depending on whether the two vortices are of equal or opposite polarities, they will gyrate around their respective equilibrium positions in equal or opposite directions.

Depending on the direction of the field, the vortex cores will either be displaced horizontally or vertically. This is also true for the single disk structure. However, due to the different chiralities necessary to create such a two vortex structure, the cores will be displaced in opposite directions. This becomes clear when looking at figure 4.17.

The displacement of vortex cores is independent of their respective polarities. Once displaced, however, the direction of gyration is solely based on polarity. Depending on core polarity and direction of the displacement field, there are several possibilities as to the intitial gyrating motion of the vortex cores. These are illustrated in figure 4.18.

It should be evident, looking at figure 4.18(a), that in the case of $p_1 p_2 = +1$ (equal polarities) the cores will rotate in such a fashion that they are out of phase by π, regardless of the direction of the applied field. We will refer to this out-of-phase rotation of vortices of equal polarity as *Mode 1*.

In the case of opposite polarities (Fig. 4.18(b)), the vortices will either rotate in such a fashion that they are both at the far right (or far left) of their respective trajectories at the same time, or such that the distance between the vortices is minimized for part of the trajectory. We will refer to these rotational patterns as *Mode 2* and *Mode 3* respectively.

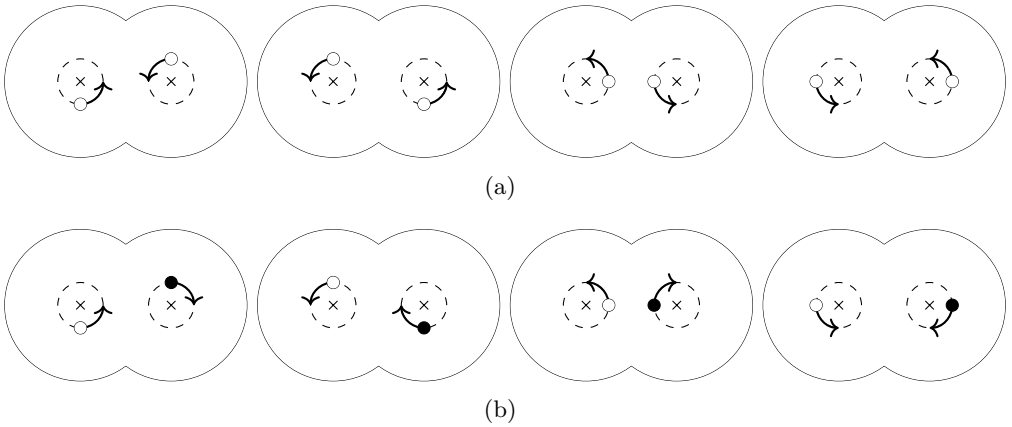

FIGURE 4.18: *Intitial gyrating motion of the vortex cores of (a) equal, and (b) opposite polarities. The displacement fields for the structures are, from left to right, in the positive* x*-direction, the negative* x*-direction, the positive* y*-direction, and the negative* y*-direction.*

As with *Mode 3*, *Mode 1* will also see the vortices rotating in such a fashion that they are both closest to the center of the two disk structure at the same time, minimizing the distance between them. *Mode 2* however, does not let the vortices minimize the distance between them. Therefore, comparing the trajectories of these different modes, it should be possible to examine how the vortices interact with one another and to test the electrostatic analogy.

4.2.2 Linear and nonlinear regimes

An important aspect of displacing the vortex in order to provoke the gyrating motion, is for which strengths of the displacement field we move into the nonlinear regime (see Sec. 4.1.5). As we wish to study the repulsive interaction between vortices, a larger radius of the gyrating motion is desired, as any alteration in the trajectories will then be easier to measure. It is thus desirable to determine a maximum value for the displacement field, for which we are still within the linear regime.

In order to determine an approximate value of the field, at which a transition from the linear to the nonlinear regime occurs, a series of simulations with gradually increasing field strengths were performed. It should be noted that the aim of these simulations was not to accurately determine a conclusive value for this field, rather to get an approximate value that would allow further simulations without the possibility of vortex polarity switching. These values are presented in table 4.1. The field strength was increased in steps of 1 mT (0.5 for one of the structures).

The fact that the transition into the nonlinear regime for the disks with a center-to-center distance of 0.4 µm occurred at a slightly lower field in the case of opposite

Center-to-center distance	Equal polarities	Opposite polarities
0.4 µm	$H_x = 3\,\mathrm{mT}$	$H_x = 2.5\,\mathrm{mT}$
0.4 µm	$H_y = 5\,\mathrm{mT}$	$H_y = 5\,\mathrm{mT}$
0.6 µm	$H_x = 3\,\mathrm{mT}$	$H_x = 3\,\mathrm{mT}$
0.6 µm	$H_y = 4\,\mathrm{mT}$	$H_y = 4\,\mathrm{mT}$

TABLE 4.1: *Field strength found to maximize the displacement of the vortex cores, without moving into the nonlinear regime.*

Mode	Horizontal diameter	Vertical diameter	Δd
Mode 1	0.241 µm	0.392 µm	0.615
Mode 2	0.296 µm	0.382 µm	0.775
Mode 3	0.221 µm	0.281 µm	0.786

TABLE 4.2: *Diameters of trajectories and Δd for the different rotational modes of vortices in two overlapping 1 µm disks with a center-to-center distance of 0.6 µm*

polarities, as compared to the case with equal polarities (2.5 and 3 mT respectively) should be addressed. The field strength increments were initially set to 1 mT. 3 mT was found to be the the maximum field strength in which vortices with equal polarities remained within the linear regime. Observing that the same was not the case for vortices of opposite polarities, additional simulations were performed with at reduced increment in field strength of 0.5 mT. Thus it is possible that the transition between the linear and nonlinear regimes actually occurs for a value of H much closer to 3 mT than to the indicated value of 2.5 mT. Any further investigation into this manner was not performed.

4.2.3 Vortex core trajectories and eigenfrequencies

The trajectories of two interacting vortices are are shown in figure 4.19. Comparing figures 4.19(a) and 4.19(b) it is evident that the distance between vortices has an impact on their respective trajectories. As a way of quantifying this impact, we introduce the expression

$$\Delta d = \frac{\text{horizontal diameter}}{\text{vertical diameter}} \tag{4.3}$$

where the diameters refer to those of the vortex core trajectory, indicated by green and pink in the plots of figure 4.19. The values of the diameters, as well as Δd for the different trajectories are presented in table 4.2

Comparing Δd for *Mode 1* and *Mode 2*, we find a relative difference of 20.6%, confirming a repulsive interaction between the vortices.

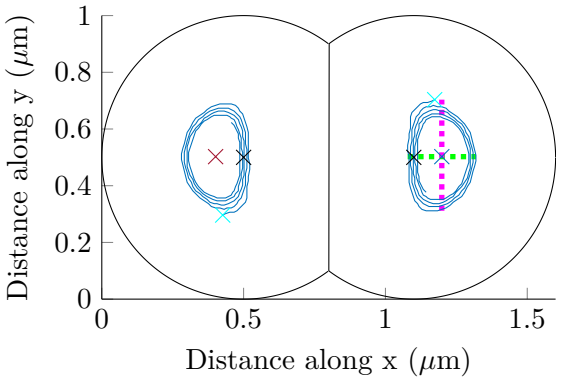

(a)

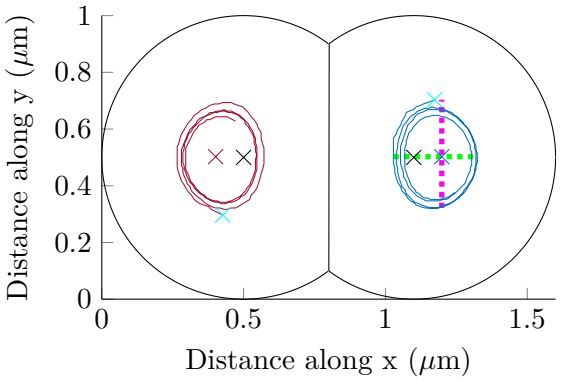

(b)

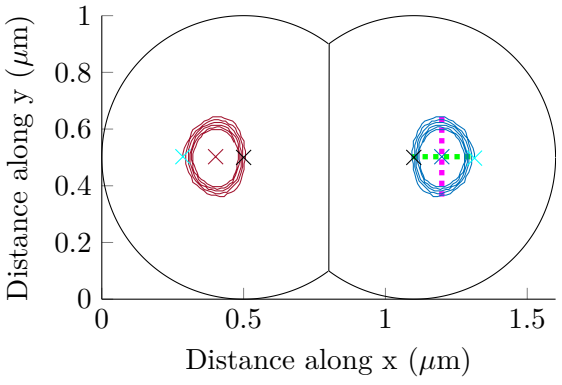

(c)

FIGURE 4.19: *Vortex core trajectories in two overlapping 1 µm disks, with a center-to-center distance of 0.6 µm, for the modes (a) Mode 1, (b) Mode 2, and (c) Mode 3. Polarity is indicated by blue (red) for $p = +1$ ($p = -1$). The vortex cores were displaced by static fields of (a) and (b) $H_x = 3\,\mathrm{mT}$, and (c) $H_y = 4\,\mathrm{mT}$.*

Mode	Eigenfrequency	Eigenfrequencies for ellipse [26]
Mode 1	90.33 MHz	204 MHz
Mode 2	73.24 MHz	96 MHz
Mode 3	109.86 MHz	264 MHz

TABLE 4.3: *Eigenfrequencies for coupled vortices extracted from the time evolution of* $\langle M_x \rangle$.

The corresponding eigenfrequencies for the gyrating motions illustrated in figure 4.19 is shown in table 4.3. These results are in good agreement with other findings, as is evident when comparing the second and third column. Quanitatively, the eigenfrequencies don't agree, which is to be expected, as the simulations performed in [26] used material parameters typical for permalloy. However, we see that the way the eigenfrequencies vary for the different modes, matches that of these other findings. Furthermore, these eigenfrequencies are close to that of a single vortex in a 1 µm LSMO disk (see fig. 4.5).

Looking at figure 4.19, it becomes evident that it is requires higher fields to displace the vortex cores vertically (Fig. 4.19(c)), as compared to horizontally (Figs. 4.19(a) and 4.19(b)). This would be natural to expect in the case of a vertical field pushing the cores towards one another, as we would expect them to resist this displacement by virtue of their repulsive interaction. In the case of the vertical field pushing the vortex cores apart from each other, however, the reason for this "reduced" displacement is not quite as self-explanatory. A rudimentary explanation can be provided by comparing the displacement to the initial magnetization states seen in figure 4.17. For a horizontal displacement field, we see that area of parallel magnetization mainly expands vertically. For a vertical displacement field, however, we observe that the area completely magnetized parallel to the field is larger. It also seems to expand more in the vertical direction, thus not contributing to displacement of the cores.

Results for simulations with a smaller center-to-center distance between the disks are presented in figure 4.20. As we are mainly interested in the difference in trajectories when the cores are both at the inner position of their circular paths at the same time, since the proximity is largest in those cases, only those results are presented here. The values of the diameters, as well as Δd for the different trajectories are presented in table 4.4.

When comparing the Δd for the trajectories in figure 4.20, we find a relative difference of 25.5%. In the structures with a center-to-center distance of 0.6 µm, this difference was found to be 20.6%. It is in other words evident that as the vortices are forced closer together, the resistive force between them increases, confirming electrostatic-like repulsion.

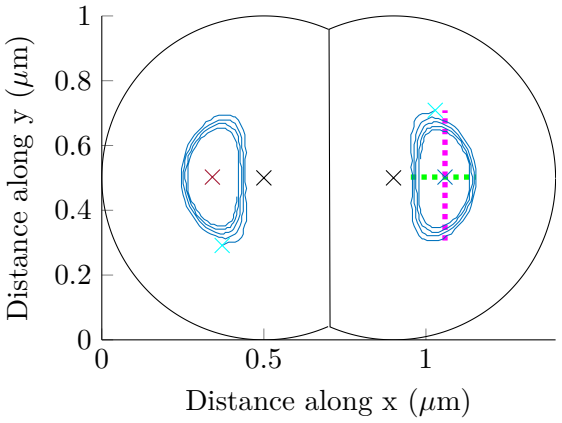

(a)

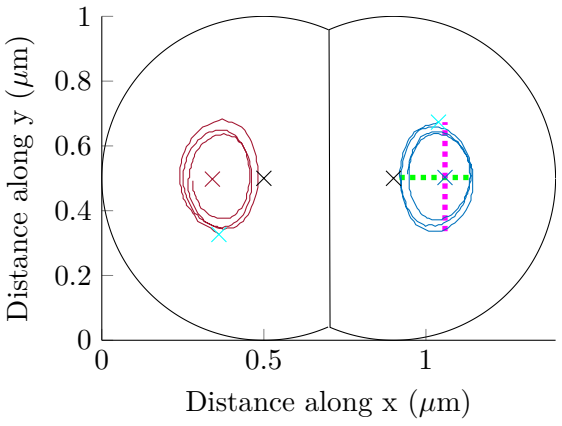

(b)

FIGURE 4.20: *Vortex core trajectories in two overlapping 1 µm disks, with a center-to-center distance of 0.4 µm, for the modes (a) Mode 1, and (b) Mode 2. Polarity is indicated by blue (red) for $p = +1$ ($p = -1$). The vortex cores were displaced by static fields of (a) $H_x = 3\,\mathrm{mT}$, and (b) $H_x = 2.5\,\mathrm{mT}$.*

Mode	Horizontal diameter	Vertical diameter	Δd
Mode 1	0.201 µm	0.402 µm	0.5
Mode 2	0.226 µm	0.337 µm	0.671

TABLE 4.4: *Radii of trajectories and Δd for the different rotational modes of vortices in two overlapping 1 µm disks with a center-to-center distance of 0.6 µm*

The eigenfrequencies of the vortex oscillations in the structure with a center-to-center distance of 0.4 µm was found to be 84.23 MHz and 64.70 MHz, for *Mode 1* and *Mode 2* respectively. These values are slightly lower than those in the case of center-to-center distance of 0.6 µm (see Tab. 4.3). This is due to the fact that a reduction in the center-to-center distance will effectively reduce the volume of the structure, thus decreasing the value of the saturation magnetization M_s. As described in section 4.1.3, the eigenfrequency will decrease for lower values of M_s, which corresponds with the results.

Chapter 5

Conclusion

The aim of this work has been to investigate the dynamics of the magnetic vortex state. Specifically the interaction between two vortices was of interest.

Investigations into the dynamic properties of a single vortex confined in a LSMO disk with a diameter of 2 µm proved to be in good agreement with theoretical predictions. The eigenfrequency of the translational mode was found to be 47 MHz.

Varying the saturation magnetization and the exchange stiffness, we see that their effect on the eigenfrequency is close to what we would expect from the analytical expression (Eq. 2.13). However, a slight deviance was observed for very low values of A. This can possibly be attributed to a reduced simulation time, resulting in insufficient oscillations around the equilibrium position to be able to accurately calculate the eigenfrequency. There is also a chance that the analytical expression is not adequate for such extreme values of A. But as the full derivation of this expression was beyond the scope of this thesis, a complete overview of its limitations proved difficult to determine.

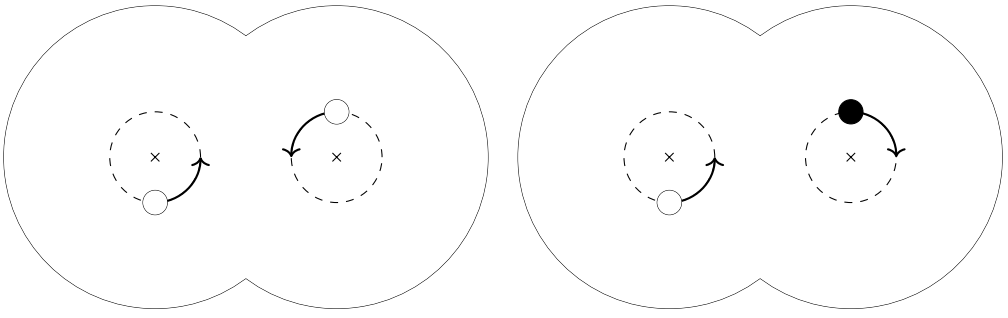

FIGURE 5.1: *Rotational modes for two vortex cores of (a) equal, and (b) opposite polarities, after an applied field in the positive* x*-direction.*

It was found that a static in-plane magnetic field can provoke three different rotational modes, depending on vortex polarity and direction of the field. For equal

polarities, the vortices rotate out of phase by π (radians), independent of the direction of the applied field. This minimizes the distance between the vortices for parts of their trajectories (see Fig. 5.1(a)). For opposite polarities, an applied field in the x-direction will produce a mode where the vortices are at the right (or left) extreme of their respective trajectories simultaneously, thus never minimizing the distance between them (see Fig. 5.1(b)).

Little research has focused on the interaction between two vortices, with regard to the electrostatics analogy described in section 2.2.4. The two different rotational modes illustrated in figure 5.1 provided a good basis for investigation of the repulsive vortex-vortex interaction by comparison of their respective trajectories. For two overlapping disks with a center-to-center distance of 0.6 µm, such a comparison revealed a difference in trajectory diameter ratio (the ratio of the horizontal to the vertical diameter) of 20.6% between the different modes. By decreasing the center-to-center distance to 0.4 µm, this relative difference was found to increase to 25.5%. These results confirm the presence of a repulsive interaction, similar to what we would expect from the electrostatic analogy.

Bibliography

[1] Y. Nakatani, A. Thiaville, and J. Miltat. Head-to-head domain walls in soft nanostrips: a refined phase diagram. *J. Magn. Magn. Mater.*, 290–291:750–753, 2005.

[2] K. L. Metlov and K. Y. Guslienko. Stability of magnetic vortex in soft magnetic nano-sized circular cylinder. *J. Magn. Magn. Mater.*, 242:1015–1017, 2002.

[3] K. Y. Guslienko. Magnetic vortex state stability, reversal and dynamics in restricted geometries. *J. Nanosci. Nanotechnol.*, 8:2745–2760, 2008.

[4] K. Y. Guslienko, K. Lee, and S. Kim. Dynamic origin of vortex core switching in soft magnetic nanodots. *Phys. Rev. Lett.*, 100:027203, 2008.

[5] G. E. Moore. Cramming more components onto integrated circuits. *Electronics*, 38 (8), 1965.

[6] M. N. Baibich, J. M. Broto, A. Fert, F. Nguyen Van Dau, F. Petroff, P. Etienne, G. Creuzet, A. Friederich, and J. Chazelas. Giant magnetoresistance of (001)fe/(001)cr magnetic superlattices. *Phys. Rev. Lett.*, 61:2472–2475, 1988.

[7] M. Riordan and L. Hoddeson. *Crystal Fire.* W.W Norton & Company Limited, 1998.

[8] W. Porod, G. H. Bernstein, G. Csaba, S. X. Hu, J. Nahas, M. T. Niemer, and A. Orlov. Nanomagnet logic (nml). In *Field-Coupled Nanocomputing: Paradigms, Progress, and Perspectives*, pages 21–32. Springer, 2014.

[9] J. Shibata, K. Shigeto, and Y. Otani. Dynamics of magnetostatically coupled vortices in magnetic nanodisks. *Phys. Rev. B*, 67:224404, 2003.

[10] R. Antos, Y. Otani, and J. Shibata. Magnetic vortex dynamics. *J. Phys. Soc. Jpn*, 77(3):031004, 2008.

[11] V. Novosad, F. Y. Fradin, P. E. Roy, K. S. Buchanan, K. Yu. Guslienko, and S. D. Bader. Magnetic vortex resonance in patterned ferromagnetic dots. *Phys. Rev. B*, 72:024455, 2005.

[12] K. Y. Guslienko, B. A. Ivanov, V. Novosad, Y. Otani, H. Shima, and K. Fukamichi. Eigenfrequencies of vortex state excitations in magnetic submicron-size disks. *J. Appl. Phys.*, 91(10):8037–8039, 2002.

[13] J. P. Park, P. Eames, D. M. Engebretson, J. Berezovsky, and P. A. Crowell. Imaging of spin dynamics in closure domain and vortex structures. *Phys. Rev. B*, 67:020403, 2003.

[14] J. Shibata and Y. Otani. Magnetic vortex dynamics in a two-dimensional square lattice of ferromagnetic nanodisks. *Phys. Rev. B*, 70:012404, 2004.

[15] P. M. Chaikin and T. C. Lubensky. *Principles of condensed matter physics*. Cambridge University Press, 1995.

[16] R. C. O'Handley. *Modern Magnetic Materials: Principles and Applications*. John Wiley & Sons, Inc., 2000.

[17] B. D. Cullity and C. D. Graham. *Introduction to Magnetic Materials*. John Wiley & Sons, Inc., 2nd edition, 2009.

[18] J. Skaar. Elektromagnetisme, 2013. Compendium used in the course TFE4120.

[19] R. Skomski. *Simple Models of Magnetism*. Oxford University Press, 2008.

[20] P. Perna, C. Rodrigo, E. Jiménez, F. J. Teran, N. Mikuszeit, L. Méchin, J. Camarero, and R. Miranda. Tailoring magnetic anisotropy in epitaxial half metallic $La_{0.7}Sr_{0.3}MnO_3$ thin films. *J. Appl. Phys.*, 110(1):013919, 2011.

[21] D. Carlton. Nanomagnetic logic. Technical Report UCB/EECS-2012-22, Electrical Engineering and Computer Sciences, University of California, February 2012.

[22] G. Hrkac, P. S. Keatley, M. T. Bryan, and K. Butler. Magnetic vortex oscillators. *J. Phys. D: Appl. Phys.*, 48:453001, 2015.

[23] A. Pushp, T. Phung, C. Rettner, B. P. Hughes, S. Yang, L. Thomas, and S. S. P. Parkin. Domain wall trajectory determined by its fractional topological edge defects. *Nat Phys*, 9(8):505–511, 2013.

[24] O. Tchernyshyov and G. Chern. Fractional vortices and composite domain walls in flat nanomagnets. *Phys. Rev. Lett.*, 95:197204, 2005.

[25] H. Beck and D. Ariosa. Vortex dynamics in the 2-d xy model. *Solid State Communications*, 80(9):657 – 661, 1991.

[26] H. Hata, M. Goto, A. Yamaguchi, T. Sato, Y. Nakatani, and Y. Nozaki. Coupled oscillations of vortex cores confined in a ferromagnetic elliptical disk. *Phys. Rev. B*, 90:104418, 2014.

[27] K. S. Buchanan, P. E. Roy, M. Grimsditch, F. Y. Fradin, K. Y. Guslienko, S. D. Bader, and V. Novosad. Soliton-pair dynamics in patterned ferromagnetic ellipses. *Nat. Phys.*, 1:172–176, 2005.

[28] G. Bertotti, I. D. Mayergoyz, and C. Serpico. *Nonlinear Magnetization Dynamics in Nanosystems*. Elsevier Ltd., 2009.

[29] What is gpu accelerated computing? `http://www.nvidia.com/object/what-is-gpu-computing.html`. Accessed: 2015-13-12.

[30] A. Vansteenkiste, J. Leliaert, M. Dvornik, M. Helsen, F. Garcia-Sanchez, and B. Van Waeyenberge. The design and verification of mumax3. *AIP Advances*, 4(10), 2014.

[31] S. Slöetjes. Simulations of micromagnetic domains. Internship Report at the Department of Electronic and Telecommunications, NTNU, 2014.

[32] K. Y. Guslienko, X. F. Han, D. J. Keavney, R. Divan, and S. D. Bader. Magnetic vortex core dynamics in cylindrical ferromagnetic dots. *Phys. Rev. Lett.*, 96:067205, 2006.

[33] K. S. Buchanan, P.E. Roy, F. Y. Fradin, K. Y. Guslienko, M. Grimsditch, S. D. Bader, and V. Novosad. Vortex dynamics in patterned ferromagnetic ellipses. *J. Appl. Phys.*, 99(8), 2006.

[34] K. Y. Guslienko, W. Scholz, R. W. Chantrell, and V. Novosad. Vortex-state oscillations in soft magnetic cylindrical dots. *Phys. Rev. B*, 71:144407, 2005.

[35] E. Kreyszig. *Advanced Engineering Mathematics*. John Wiley & Sons, Inc., 9th edition, 2006.

Appendix A

Scripts

A.1 Fourier transform

```
function [] = plotFFT(table)

    %Get values from MuMax3 data table
    Mx = table.mx__;
    time = table.x_T_s_;

    runTime = time(length(time));
    saveInterval = runTime/length(time);

    Fs = 1/saveInterval; %Sampling frequency
    L = length(Mx);
    nfft = 2^(nextpow2(L)+4); %Length of FFT

    %Do FFT
    mxFFT = fft(Mx, nfft);

    %FFT is symmetric, throw away second half
        mxFFT = mxFFT(1:nfft/2);

    % Calculate magnitude of FFT
    mx = abs(mxFFT)/sqrt(L);

    % Frequency vector
    freq = (0:nfft/2-1)*Fs/nfft;

    %Find peak values
        [mxPeakValue, mxPeakIndex] = max(mx);
        peakXIndex = freq(mxPeakIndex);
        peakYIndex = mxPeakValue;

    %Plot result
    figure
    plot(freq*1e-6, mx);
        xlim([0 4*peakXIndex*1e-6]);

end
```

A.2 Locating vortex core positon

```
function [maxValIndices, polarity] = findCorePosIndices(Mz, numOfCores)
    %Input: Mz: dataz field when importing .ovf-files with oomf2matlab
    %       numOfCores: number of vortices to locate
    %Output: maxValIndices: vector with indices referring to row and column in the grid
    %        polarity: vector containing the polarity of each core

    maxValIndices = zeros(numOfCores, 2);
    polarity = zeros(numOfCores, 1);

    absMz = abs(Mz);

    for i = 1:numOfCores
        [maxVals, rowsContainingMax] = max(absMz, [], 2);
        [maxValue, columnIndex] = max(maxVals);
        maxValIndices(i, :) = [columnIndex, rowsContainingMax(columnIndex)];
        absMz(columnIndex-1:columnIndex+1, :) = 0;

        if Mz(columnIndex, rowsContainingMax(columnIndex)) > 0
            polarity(i) = 1;
        else
            polarity(i) = -1;
        end

    end

    [maxValIndices, sortIndex] = sortrows(maxValIndices);
    polarity = polarity(sortIndex,:);
end
```

```
function [] = plotTrajectories(numOfCores, initMagData, magData)

    %Get maximum x- and y-values, and position matrices
    xmax = initMagData.xmax;
    ymax = initMagData.ymax;

    %Find position of vortex cores at equilibrium (m_initial)
    initMz = initMagData.dataz;
    [initCoreIndices, initPolarity] = findCorePosIndices(initMz, numOfCores);
    initCorePosX = xpos(initCoreIndices(:, 1));
    initCorePosY = ypos(1, initCoreIndices(:, 2));
    initCoreStruct = struct('x', initCorePosX, 'y', initCorePosY, 'polarity', initPolarity);

    %Initialize struct
    corePositions = struct([]);

    for i = 1:length(magData)
        Mz = magStruct(i).dataz;
        [coreIndices, corePolarity] = findCorePosIndices(Mz, 2);
        corePosX = xpos(coreIndices(:, 1));
        corePosY = ypos(1, coreIndices(:, 2));
        tempStruct = struct('x', corePosX, 'y', corePosY, 'polarity', corePolarity);
        corePositions = [corePositions, tempStruct];
    end
```

```
%Additional code for creating disk outlines
diameter = ymax;
r = diameter/2;
overlap = 2*ymax - xmax;
centerDist = diameter - overlap;

ang = 0:0.01:2*pi;
xp = r*cos(ang);
yp = r*sin(ang);

%Left disk
x1 = r + xp;
y1 = r + yp;

%Right disk
x2 = x1 + centerDist;
y2 = y1;

%Exclude outline for part of disks overlapping
ex1 = find(x1 >= r + centerDist/2);
ex2 = find(x2 <= r + centerDist/2);
x1(ex1) = [];
y1(ex1) = [];
x2(ex2) = [];
y2(ex2) = [];

%Plot everything
figure
hold on

for i = 1:numOfCores
    for j = 1:length(magStruct)
        %Plot positions with color corresponding to core polarity
        if corePositions(j).polarity(i) == -1
            plot(corePositions(j).x(i), corePositions(j).y(i), 'r.');
        else
            plot(corePositions(j).x(i), corePositions(j).y(i), 'b.');
        end
    end

    if initCoreStruct.polarity(i) == -1
        plot(initCoreStruct.x(i), initCoreStruct.y(i), 'rx');
    else
        plot(initCoreStruct.x(i), initCoreStruct.y(i), 'bx');
    end
end

%Disk outlines
plot(x1, y1, 'Color', [0.5,0.5,0.5]);
plot(x2, y2, 'Color', [0.5,0.5,0.5]);

%Define axis properties
axis equal tight
ax = gca;
```

```
    xAxis = 0:0.2e-6:xmax;
    yAxis = 0:0.2e-6:ymax;
    ax.XTick = xAxis;
    ax.YTick = yAxis;
    ax.XTickLabel = xAxis*1e6;
    ax.YTickLabel = yAxis*1e6;
    xlabel('x (\mum)');
    ylabel('y (\mum)');
end
```